Response to Reviewer 1

Spectral attenuation of gravity wave and model calibration in pack ice Cheng et al.
tc-2019-290

Authors' response:
We appreciate the reviewer's careful reading and the support of this study very much. A revised manuscript has not been prepared at the time due to the editor's request. We have revised the manuscript to respond to all of the issues raised by the reviewer. The review comments are listed below in black, and our responses are in red.

In their manuscript „Spectral attenuation of gravity wave and model calibration in pack ice", Sukun Cheng and colleagues present results of an analysis of wave energy attenuation based on data obtained from a set of SAR scenes from the Beaufort Sea. The analysis includes: (i) derivation of spectral wave characteristics in the area of interest, divided into two sub-regions with different ice types and morphology, (ii) computation of linear attenuation coefficients for a large number of pairs of points located in both sub-regions, and (iii) calibration of parameters of two selected models of wave attenuation, by Fox and Squire, and Wang and Shen, to the observed spectral attenuation. The manuscript also includes a discussion of possible sources of errors in the analysis, data deficiencies, as well as a more general discussion of problems with model calibration related to a large number of unknown coefficients and with the fact that a multitude of different physical mechanisms contribute to the net attenuation observed in the field. It is relatively easy to point out limitations of this type of analysis, but – as the Authors rightfully remark – our limited understanding of the processes involved, combined with limited availability of data for model calibration and validation, restrict our ability to develop complex, physics-based models and justify development of simplified, but practically applicable parameterizations (like those implemented in the WW3 wave model). Therefore, in my opinion, the work presented in the manuscript is very valuable and has several aspects practically relevant for spectral modeling of wave propagation and dissipation in sea ice. I think that the results are worth publishing in "The Cryosphere". My comments on the manuscript are listed below.

General comments:

1. The text of the manuscript contains a lot of (mostly small) grammar, punctuation and other language mistakes and should be carefully corrected before publication.
   We have cleaned up the language mistakes.

2. I'd suggest modifying the title of the paper. I understand the Authors wanted the title to be short, but in my opinion they over did it. "Model calibration in pack ice" – what kind of a model? It might mean anything. I'd also suggest changing "gravity wave" to "gravity waves".
   The title is revised as "Spectral attenuation of ocean waves in pack ice and its application in calibrating viscoelastic wave-in-ice models"

3. The location of FAL – and its very existence – is crucial to the analysis presented in this paper. The Authors first introduce this term on page 3 (lines 75-76), suggesting that it was used (or defined) by Stopa et al. (2018b). It should be Stopa et al. (2018a) – see also my technical comment no. 1 below. But, more importantly, even if that information is provided in the previous papers, I'd suggest adding it to the present manuscript as well: how was the position of FAL determined? How does the ice cover differ on both sides of the FAL-line? In the present form, the FAL seems rather "mysterious". For example, further on page 3 we read: "…the FAL (black dots) presumably marks the separation between discrete floes and a semi-continuous ice cover with dispersed leads". (A bit further, in line 120, again: "presumably a semi-continuous cover".) Presumably? Does it mean those features cannot be unambigously identified in the analyzed images? How then was the position of FAL determined? What was the criterion? What is the uncertainty

associated with the location of FAL? Very importantly: was the location of FAL determined independently of any information on wave characteristics? Could the authors add a figure showing fragments of the analyzed images on both sides of FAL (not necessarily in the main text, but in the supplement)?To make it clear: I'm not criticizing the analysis nor the way FAL was defined/identified, but the presentation in the manuscript.

We have included the explanation of the first appearance of leads (FAL) as Appendix A. "Appendix A

The definition of the first appearance of leads was introduced in Stopa et al. (2018b). Here we provide more details of the methodology used. The SAR sea surface roughness imagery in Figure 1 of Stopa et al. (2018b) are divided into 5.1x7.2 km subimages with a 50% overlap of adjacent subimages in the range-azimuth domain. Each subimage contains 512×512 pixels. The FAL location for each range-position is defined as the minimum azimuth position where large-scale ice features were detected. A detection of large-scale ice features is applied on each SAR subimage as the following. We first compute a one-dimensional spectrum of the SAR subimage to produce an image modulation spectrum. The spectrum is then normalized by the maximum energy contained in wavelengths from 100 to 300 m (the wavelength range of the dominant sea state for this event). When the ratio of the average of the normalized image spectra with wavelengths in the range of 600-1000 m and the dominant ocean-wave wavelength range from 160-220 m exceeds 0.8, we deem that there is a "large-scale" feature such as lead within the image. Figure A1 shows two representative examples of detecting ice leads from SAR images captured before and after the FAL. From the criterion above, there is no leads in the top case, but leads are found in the bottom case. Also notice the change in the probability distribution of the roughness: the mean value changes (lower in the non-lead case compared to the lead case) and the standard deviation (lower in the non-lead case compared to the lead case).

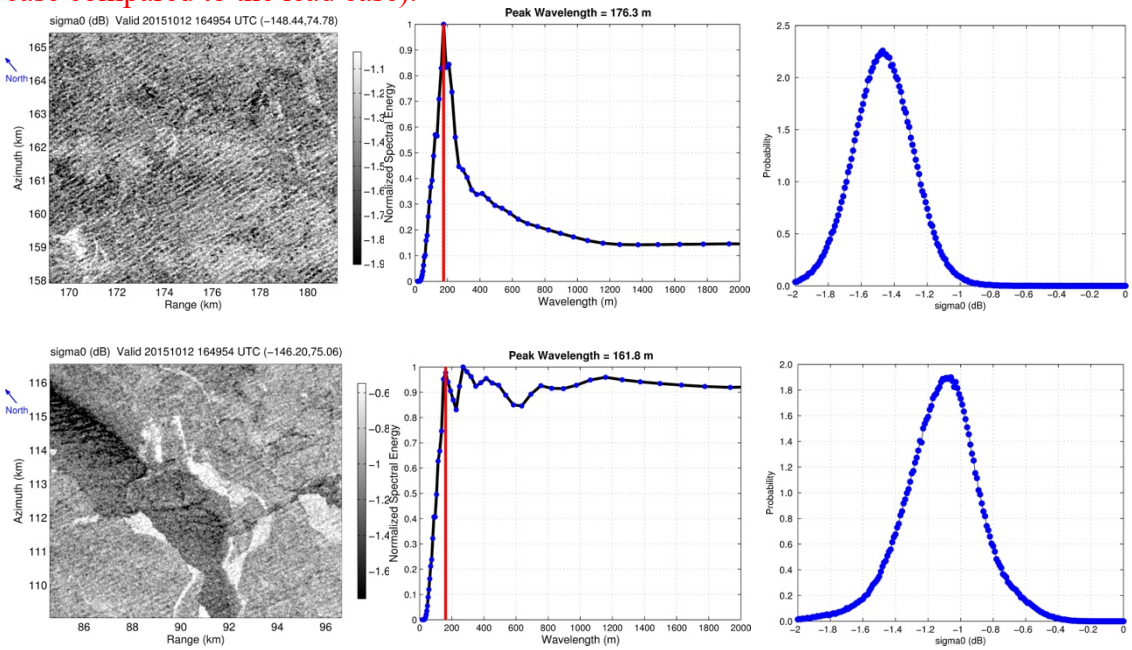

Figure A1. Illustration of the process to determine the FAL using two representative SAR subimages. (left) Surface SAR subimage roughness for a case located before the FAL (top) and a case located after the FAL. (middle) Normalized spectral energy (normalized by the maximum energy within the 100-300 m wavelengths) of the SAR subimages where the red line indicates the dominate wavelength. (right) The probability density function of the SAR roughness (backscatter or sigma0 of thermal noise in the SAR imagery) for the two cases."

As far as I know from other studies (I'm not an expert in satellite data analysis), the satellite algorithms used to determine ice concentration and thickness perform relatively poor in thin, "new" ice types (frazil, grease, pancake ice).
Could the Authors comment on the reliability of the concentration and thickness maps (Fig. 1b,c) in the region south of FAL, where the thickness is 10 cm or less? Is the apparent west-east gradient of ice concentration and thickness in that region really present or is it possible that in fact it is a change of ice type? Those questions are important for some aspects of the analysis, for example, in line 118, where the Authors say that the wavenumber "varies with ice concentration but is insensitive to ice thickness variation…".
To explain the use of AMSR2 and SMOS, we have added the following comments in lines 220-221 in the mark-up manuscript.
"As shown in Cheng et al. (2017) (Supporting information Figures S6 and S7), these two ice products compared the best with in-situ observations in the MIZ. Their accuracies in the pack ice zone are uncertain."

Response to Reviewer 2

Spectral attenuation of gravity wave and model calibration in pack ice Cheng et al.
tc-2019-290

Authors' response:

We appreciative very much the careful reading of the reviewer. Whose suggestions should make this manuscript much more readable to a broader range of audience in polar science. A revised manuscript has not been prepared at the time due to the editor's request. We have revised the manuscript to respond to all of the issues raised by the reviewer. Our replies (in red) to the reviewer are added under each of the specific comments (in black).

This paper documents a study of the attenuation of sea surface gravity waves by sea ice. The study involves the use of Sentinel 1A SAR imagery to extract first a wave number direction spectrum within a region of thin sea ice in the Beaufort Sea. Physical laws are introduced that use the SAR data to get the apparent wave attenuation and wave attenuation due to ice effect. A calibration scheme is then introduced that takes the modeled wave frequency spectrum, generates the wave attenuation due to sea ice, and then compares these values to the data. The calibration scheme is used to find optimal model parameters of the shear modulus and molecular viscosity to best reproduce the observed conditions. Optimal values are presented along with a detailed discussion of how they compare to previous studies. The detailed analysis of wave attenuation required to calibrate the wave model has then also been used to discuss the physics in play. A particular emphasis here, and through the analysis is on differing characteristics within the ice pack before or after lead formation. The authors do well to show the role of their work within the science of the highly complex system of wave ice interaction and the benefits of using the analysis and calibration presented. After the authors address points i have below regarding the documentation of the papers methodology I suggest it is fit for publication.

We thank the reviewer for the support which is very encouraging.

Whilst this paper well documents the technical parts of data analysis and model calibration, and thoroughly discusses the success, limitations and implications of their results, it is severely lacking in any general description of the methods used. I had to read the entire paper, and all the specific details of the methods before I could understand the general incentives and methods of the study. I have suggestions below for how to improve the paper to address this. Once I had worked out what methods of the paper were the various sections of the paper fell into place and the science behind the paper was well founded and thoroughly discussed. However, I still have some key questions.

1) The paper does not clearly explain the reader the format of the data used and the extent of analysis performed for this study. Do you take the wave energy spectrum from Stope 2018b or the wave number direction spectrum? Or you start with the raw SAR imagery and repeat the same analysis as before? I spent much of section 2 asking myself this. Also the format of the introduction adds to this confusion, whilst it starts with 4 paragraphs of overview, paragraph 5 is neither an introduction to the area of interest, or a description of the data used in this paper. The rest of the paper has a similar ambiguity between the data sources for this study, the data processed as part of this paper and previous studies that are being cited for comparison.

2) There is little description within the paper of what is being documented by each section. The brief outline on lines 103-109 is again ambiguous to what is being performed. For example 'site description and wave characteristics are depicted in section 2' does not inform me as to whether section 2 contains description of the data used in the study and how you processed it, a summary of previous studies of the region and what they found, or even a description of a model run of the region. Section 2 itself starts immediately with a definition of kr, which is clearly done, but there is no description at all of whether kr in this study is an original data source collected by the study or a previously collected data that is being analyzed here. This lack of overview is present in near all of the technical sections with the paper. I suggest adding a clear paper overview of the form; data was obtained from (here, here, etc) that we analyze thusly to extract this information. We then ran these models and using this scheme and the previously documented data we calibrated these parameters. This information also needs to be clearly defined at the beginning of each

section. Once I had worked out this information for myself I was easily able to understand the technical parts of the study, which are well written.

3) There are two key values used in this study, apparent wave attenuation and the wave attenuation due to ice effect. The notation for these needs to be changed. kr is a wave number spectrum, alpha is the associated wave attenuation, but ki is just a wave attenuation whilst previous notation leads me to think it will also be a wave number. While the methods used to get these values are documented, there is no physical description of what these values represent and why you are interested in them. A paragraph in the introduction introducing these physical values, and the other values considered in this paper (dominant wave number, wave energy spectrum for example) will greatly help a non-specialist reader. Section 3 needs an introduction explaining the differences between kr and ki, and as mentioned before, the data you use to obtain these values. Also the wave attenuation due to ice effect ki and ki^m need to have clearer definitions. I see that you have used ki as the modeled attenuation, and ki^m as that data derived value. This notation needs adjusting, the use of superscript m to define the value that is not modeled is confusing. Section 3.2 will benefit from a definition of ki at the beginning, as currently the reader has to wait till the end of the section to understand what the aim of the presented method is.
4) I suggest that the introduction section needs restructuring and expanding upon. Currently there is one paragraph on the place of wave sea-ice interaction within climate science and then a very technical description of one wave model. The paper would benefit from having first the next paragraph that explains the uses of wave forecast models, and then the technical description of WaveWatch follow. The final paragraph of the introduction needs to moved to a dedicated data description and expanded upon. It is currently unclear what SAR data used in this study is new and what has been previously published. If the SAR observational data and analysis or processing has been previously published, then a clear section citing this publication and describing the data is needed. If there is novel data work in this study then this needs to be clearly stated and the technique and data clearly described.

We apologize for the lack of sufficient details. Several major changes have been made in the final revised manuscript to address the four concerns raised above:

- Modify and expand section 2 to include all data and site description.
- Add explanation particularly to the dataset used and the analyses done in the present study.
- Clarify notations, especially the wavenumber and attenuation rates which are now defined in the Introduction.
- Revise Introduction, and the beginning of each section and subsection to clearly describe the purpose of each section.

The specifics are given below.

Specific edits:

14 ‘wave propagation’ this is the first sentence in the paper. Please be more explicit in which waves you re discussing. Consider an additional sentence introducing ocean surface gravity waves 14 ‘fall 2015’ please give a more accurate time. The study is for a single day i believe.
We have specified “ocean waves” in the title and throughout the manuscript whenever necessary. We also added the date to the SAR dataset.

21 - 24 this sentence is very long. I had to re-read several times to understand what became lower where. Consider splitting.
The long sentence here and several other long sentences throughout the manuscript are split into short and clear sentences in lines 23-26 and the abstract have been modified in the revised manuscript.

35 These citations are 10+ years old now, the reduction and predictions have changed a lot in these 10 years.
Some recently published references have been added in the introduction in line 59.

43 Wavewatch is first introduced with a very technical description. Can you first give an overview of Wavewatch? Its uses and the incentives behind its creation. A brief description of its main physical constructs will also be useful to the reader. The ice effects as modeled by WaveWatch are described here, but I’d like to see how these ice effects sit within the whole model.

54 An introduction into how wave forecast models work would be useful here. I'd like to know how to use a wave forecast model in general, then I can better understand the context of your work in the wave sea-ice interaction aspect.
A brief description of WAVEWATCH III have been added to the second paragraph in the introduction section from line 67.

58 Here and above you mention IC3 (and IC5). You mention that they both store and dissipate mechanical energy but what are the differences between them.
The difference between IC3 and IC5 have been explained in the original version. They both describe the ice cover as a linear viscoelastic material, but IC5 also uses a thin-plate assumption while IC3 does not. We emphasise this point in the revision in lines 84 - 88.

77 This next paragraph needs moving to a dedicated data section. Within this section it needs to be made clearer what data was used as part of this study and why. Also I find it difficult to tell from this paragraph which data was collected together in a previous study and which data was brought together for this study. Those which were brought together here needed to be expanded upon. The benefits and limitations of each data need to be better discussed.
Currently the novel method of Ardhuin 2017 and Stopa 2018a is well described, as are the reasons for its use in this paper. However there is less description for the Buoy and ice concentration data. Due to the data all being plotted together in figure 1, I am assuming that this combination of data sources is novel for this study. If this is the case please state so, and explain why the data have been chosen. If however these data have been combined before (which then explains why they are described in the introduction) then citations/descriptions of findings are needed.

We have re-organized section 2 to include all data and site description, including the paragraph in the introduction regarding Figure 1. The following points are added.

a) The data set from Stopa et al. (2018b) was used as the starting point of this study. We have specified the additional analyses performed in the present study in the Abstract, Introduction, and Data description section.
b) The data from buoys and the ship shown in figure 1(a) are not used in this study. These data sources are in the marginal ice zone with mostly pancake ice studied in Cheng et al. (2017). Showing these locations in figure 1(a) contributes to a big picture of the SAR imagery.
c) The AMSR2 concentration and SMOS thickness data have been used in several publications in a special issue of Journal of Geophysical Research: Oceans regarding the "Arctic Sea State and Boundary Layer Physics Program". An overview of the program is in the reference list of this manuscript: Thomson et al. Overview of the arctic sea state and boundary layer physics program, Journal of Geophysical Research: Oceans, 123, 8674-8687, 2018. This reference is included in the manuscript.

Figure 1 There is no (a) label in the figure. Can you show on pane (a) how (b and c) colocate?
We have added symbol (a) in figure 1(a). The panels (a)(b)(c) are in the same coordinates. Particularly, the vertical range in panel (a) is from 0 to 750 km. While in panels (b)(c), the vertical range is from 450 to 750 km. Hence it is straightforward to collocate them.

106 What is the methodology of calibrating IC3? Is it used extensively in this paper? If it is then a summary of the equational from is needed. If this is complicated then consider an appendix for the equations. If it is still too complicated then a paragraph explaining how it works with relevant citations is needed.
Section 4 describes the methodology of calibrating IC3 and IC5 from line 525. In general, to obtain the "best fit" parameters, it uses an optimization method to minimize the difference between measured and model data. Details are given in the revised section 4.

Next: a full description of wave energy spectrum E(f,theta) is needed. Ether the equational form of E() needs to be added, or how it is produced by the model and how it is extracted from the data set. The source of the various E() used in this paper is a current theoretical hole for me when reading it. As it is a key value for methods of this paper, consider a paragraph in the introduction explaining how the energy spectra is calculated from observations and treated within the model you are calibrating. Some background

science on ocean surface gravity waves are described, including what the wave energy spectrum is would be a useful inclusion for this paper.
Sorry for this confusion. Since E(f,theta) is not used in the study, thus removed in the revision. In this study, we only use wavenumber-direction spectrum from Stopa et al. (2018b) as clarified at the beginning in section 2. This study doesn't involve the process of retrieving the wave energy spectra from the observations.

Also: At this point in the paper I don't want to have to dig into section 4 to discover what modification you have had to make to the methodology of Cheng 2017. At this point I flipped to section 4 and searched for both the 'Cheng' citation and the string 'IC3' within the paper and it was still unclear to me how the methodology of Cheng 2017 worked, why you had to modify it and what those modifications are. A description of all these aspects of this study is needed, either here, or at the beginning of section 4
I started reading this paragraph hoping to understand the incentives and aims of this study and what methods were used. The paper is unlikely to have been written in a linear fashion, but please remember that the reader will read it in a linear fashion, and is likely to be unaware of all the previous work on this topic, the data you are using, the model you are calibrating and the techniques you are using to calibrate it.

We fully understand the problem the reviewer mentioned. To read a paper we also often need to go back and forth, instead of linearly. To help the readability, we have revised the Introduction to better describe the structure of this manuscript. Overviews of each section are also added at the beginning of sections 2, 3, 4 and 5.
The reference to Cheng et al. (2017) is necessary in the Introduction because both the present and the 2017 study share the same goal: to calibrate wave-in-ice models so that they can be used in global models such as WAVEWATCH III. It has been a big challenge to conduct such calibration due to lack of data. We used data in mostly pancake ice fields in the 2017 study. We are very fortunate that shortly after that we have the SAR data in the pack ice zone, so that we could expand the calibration to a different type of ice cover.
The calibration is performed by minimizing the theoretical attenuation over a spectrum of wave components with the measured data. The best-fit parameters are the calibrated model parameters. The wave-in-ice models, including IC3 and IC5, are all in terms of attenuation-frequency. Hence to do this optimization the most straightforward way is to use the attenuation-frequency data. In the 2017 paper we used buoy data. They were based on time series, hence automatically in attenuation-frequency form. In the present study the spectral attenuation derived from SAR data is in terms of wavenumber. Hence additional steps are required to map the attenuation-frequency results from the theoretical models to the attenuation-wavenumber space. This is non-trivial, but an intricate point that needs to be pointed out. We have revised methodology better in the relevant section. The Introduction only briefly mentions that the methodology is not as straightforward as in the 2017 study.

110 I am assuming that this section is a description of the data used in the study. However you give no indication of this in the text. I start by asking 'the wave number spectrum retrieved from where?'. This does not get answered, so the following information is very difficult to understand.
112 This range suggests you are talking about figure 1? I should have to work this out myself.
113 fitted to which E(f,theta) from where?
115 I can't understand the direction sum of E(kr,theta) when you have not described where kr comes from and what E(f,theta) is and where that comes from. Was there a previous analysis performed to get E(f,theta)? Was that done as part of this study or previously?
117 Again I am asking whether this work of extracting kr,dominant is from this study. Was it previously done as part of Stopa 2018a/b ? Please inform the reader what work was done with the data for this study.
We have revised section 2 to address the issues above. See lines 160 – 173.

118 Difficult to see the variation with concentration in the figure.
The relationship between the dominant wavenumber and ice concentration and thickness have been revised in lines 223 – 227.

120 Again difficult to see the decrease with kr on the figure. Also it is unclear what you are referring to with 'wave propagation direction'.
The dominant wavenumber $k_{r,dominant}$ is indicated by the cell colors. Since the wave energy $E(k_r, \theta)$ is a two-dimensional quantity, each of these wavenumbers including the dominant one has a directional

energy spectrum $E_{kr}(\theta)$. The main direction with contains most of the energy as described in the first paragraph of section 2 is shown by the arrows in the figure 1(a). Hopefully the revision clearly explains these points.

122 what is the meteorological convention?
The definition has been added in line 238.

126. Please give a value here for lambda_c and/or the associated limit for kr.
Because the azimuth cutoff λ_c is estimated from the SAR image, λ_c changes at different locations. Stopa et al. (2018b) gave two examples of λ_c at different locations. That is, $\lambda_c \approx 50$ m at the drifting buoys (blue dots in figure1(a)). While at the AWAC located further into the sea ice (black asterisk in figure1(a)), $\lambda_c = 125$ m estimated from SAR image but $\lambda_c = 60$ m estimated from AWAC measurement. Thus, k_r is limited by $k_r \leq \min(2\pi/\lambda_c, 0.045\mathrm{m}^{-1})$ in line 300.

135 Is the frequency f estimated for all kr?
f and kr are related through the open water dispersion relation as mentioned in lines 310-311.

Section 3
Again this section really needs an introduction. I had to read the whole paper before I could make sense of it. Even so I still have some major questions that are easily answered by reading the paper.
We have revised section 3 by adding a brief introduction in the beginning of the section and subsections.

157 please define the 'Pearson correlation coefficient'.
The definition has been added after 'Pearson correlation coefficient' in lines 355-357.

196 Power spectral density of what? I see this is mentioned in the figure, but please also define it in the text.
We discuss about the power spectral density of wave energy. The mathematical definition of has been added after the power spectra density in line 418.

Figure 4. It would be nice to have an overlay square in figure 1 showing how the left column of figure 4 aligns.
Because the left panel in figure 4 is in longitude-latitude coordinate system, but figure 1 is in the range-azimuth coordinate system, it makes sense to add boxes in figure 1(a), but it would make the figure too messy. Thus, instead of drawing an overlay square in figure 1(a), we redraw the latitude lines corresponding the longitudes mentioned in figure 4 to help readers identify the three subregions of figure 4 in figure 1.

Please also note in the caption that the centre column is generated by pairs of data, whilst the rightmost comes from individual points.
In the right column, data of power spectra density (PSD) curves are averaged values rather than from individual points direction. Specifically, we collect the PSDs from the end locations of pairs shown in the left column. These data are averaged values per 0.1 degree in latitude. It has clarified in the revision in lines 419-420.

224-229 I suggest that a version of this paragraph come at the beginning of the section. This would much ease the reading of this paper. Here I can understand clearly which values you are obtaining from where, why you chose them and what you intend to do with them. However the picture is still not entirely clear. This style of explanation is needed for every section and sub section.
The suggested brief introductions have been added to the beginning of sections 2 to 5.

259 and figures 3 and 5. A better description of these two figure and what you wish to show with them is needed. The caption for figure 5 is not sufficient. Saying that alpha vs kr is similar to ki^m vs kr is misleading, as alpha and ki^m are not similar physical quantities.
The caption for figure 5 has been extended in line 521-524.

266 Here you say that kr and ki re solved for, but elsewhere in the paper kr is given as a data source whereas ki is a model variable. Is kr now referring to something else?

Definition of kr and ki have been added in lines 89-92. The difference between measured and theoretical kr are redefined in line 574 – 577.

278 k = kr + i ki, how are you combining a wave number from data and an attenuation factor?
Idem

286 You have now introduced kr^m. What is this symbol for. The m would indicate 'model' but the opposite is true for ki. However previously kr was from a data source. Please clear up all the ki kr notation. Avoid using ^m if you're not going to use it to indicate 'model' Equation 6 Is the subscript 2 supposed to be an exponent? If not what function does it refer to?
Same as above, we have cleaned up the notations throughout the manuscript.

366 I find the discussion of ki here confusing due to the mixed notation used. Why not ki^m? Also here you talk about ice effect wave attenuation, but earlier you talk about kr,dominant which is a wave number. Please can you clear up the notation for these.
Idem

279 is the alpha here the same as in equation 1? Are you using alpha from the SAR data source in these equations to calibrate the model? If yes, then clearly say so, if not, then an alternative notation is required.
Sorry for the confusion. α here is not the same as in Eq. (1). Letter 'a' has been used in Eq. (5) and its description to avoid confusion. It has been corrected in section 4.1.

280 This sentence is an important one for this paper and needs to be clearly stated in the introduction.
This information has been included in the rewritten last paragraph of the Introduction in lines 137-154.

284 This information would be better suited at the beginning of section 4, before equations 5.
We have added the extra text in the suggested position in lines 526 – 529.

285 are you actually running WaveWatch as part of the calibration scheme? If so which out put variable are you taking for the calibration? I am assuming that you take the model out put frequency spectrum f, and use the relevant equations from 5 to create the required ki kr.
WaveWatch III (WW3) is not used in this analysis. But we use the governing equation (which is a general one in all global wave forecast models) in WW3 to extract the wave attention coefficient due to the ice effect. To do so, we need to calculate all other source terms S_{in}, S_{ds} , S_{nl}. They are based on the formulations given in the WW3 manual. In addition, we also need to argue that time derivation in this governing equation is negligible as discussed in the manuscript. A brief description of WW3 is included in the second paragraph in the Introduction.

308 I would like to see a figure of the clustering of retrieved parameters. The table plus description does not give enough information.
Moving figure S2 and S3 to the main context might make a very long manuscript. We think the scatter plots are lower level information than the other figures. Hence we keep them in the supplemental material.

314 Ah I see the scatter plots are in the supplementary material. Idem
324 Again put the scatter plots here, they are interesting. Figure 6. Idem
They would be a worthwhile inclusion in the main paper Table 1. Please expand the caption to say what these numbers are. They are the results of the model calibration I assume?
The caption of table 1 has been revised accordingly in line 640.

311-312 Sentence unclear please revise
We have revised the text to address this issue, see lines 625-631.

Pane b illegible and either needs redrawing in color, omitting 90% of the lines, or even not including in the paper.
Because hundreds of lines are superimposed in panel b, it looks like a black band. The band shows the wavenumber range predicted by the WS model, implying the validity of the model predicted wave dispersion using the calibrated parameters. We could use a broad band to show the same information, but it would lose some details such as the fluctuations of the curves, if the fluctuations are outliers or general, and the number of cases studied. We note that their fluctuations are within a very small range less than 5%.

Caption you mention ‘the data’ plotted in plot a, which data? from where? section 3 I guess.
The caption in figure 6 have been revised in lines 678.

350 It is important to also mention here the limitations of using a numerical (or a more specific description of the algorithm used) parameter search/optimisation scheme. For example: no. minima for equation 6 could be found for the data at these locations.
The issue of implementing the numerical algorithm have been added in lines 684-685. This genetic algorithm is commonly used for global optimization.

394 You here introduce a data mask, though this was not previously mentioned. Does it relate to the previous sentence on data quality? In which step of the data processing was this mask used?
Since the data ‘mask’ is not used and caused confusion in this study. This sentence has been deleted.

399 Which function are you talking about? Equation reference?
It is referred to the objective function in the model parameter optimization, i.e., Eq. (6), which has been clarified in line 759.

438 Can you point me back to the results to show the difference in dispersion.
It is shown in the right panel in figure 6 and figure S4 as mentioned in line 808-809.

Appendix I suggest moving the appendix to the main paper section. The results here appear to be as worthwhile as others discussed. Are these results from another study and you include them in an appendix for reference?
We note that in the revision Appendix A has been inserted to introduce the procedure of retrieve SAR data in Stopa (2018b) due to the suggestion from another reviewer. Hence Appendix A becomes Appendix B in the revised manuscript.
The new Appendix B shows another method in determining the wavenumber-dependent attenuation, to compare with the analysis of the attenuation of the significant wave height shown in Stopa et al. (2018b). The method in Appendix B is different from the one in section 3. The obtained attenuation rate represents an average attenuation over the entire latitude domain covering different ice conditions, thus, cannot be used in calibration for different ice types in section 4. Therefore, bringing the appendix to the main body could be distracting to the focus of this study.

Spectral attenuation of ocean waves in pack ice and its application in calibrating viscoelastic wave-in-ice models

Sukun Cheng[1,4], Justin Stopa[2], Fabrice Ardhuin[3] and Hayley H. Shen[4]

[1]Nansen Environmental and Remote Sensing Center, Bergen, Norway

[2]Department of Ocean and Resources Engineering, University of Hawaii, Mānoa, HI, USA

[3]Univ. Brest, CNRS, IRD, Ifremer, Laboratoire d'Océanographie Physique et Spatiale (LOPS), IUEM, Brest, France

[4]Department of Civil and Environmental Engineering, Clarkson University, Potsdam, NY, USA

Correspondence to: Sukun Cheng (sukun.cheng@nersc.no)

Three key points:

1. The spatial distribution of wavenumber and spectral attenuation in pack ice are analyzed from SAR retrieved surface wave spectra.
2. Spectral attenuation rate of 9~15s waves varies around $10^{-5}m^2/s$, with lower values in thicker semi-continuous ice field with leads.
3. The calibrated viscoelastic parameters are greater than those found in pancake ice.

Abstract. We investigate a case of ocean waves through a pack ice cover captured by Sentinel-1A synthetic aperture radar (SAR) on 12 October 2015 in the Beaufort Sea. The study domain is 400 km by 300 km adjacent to a marginal ice zone (MIZ). The wave spectra in this domain were reported in a previous study (Stopa et al. 2018b). In which, the authors divided the domain into two regions delineated by the first appearance of leads (FAL) and reported a clear change of wave attenuation of the total energy between the two regions. In the present study, we use the same dataset to study the spectral attenuation in the domain. According to the quality of SAR retrieved wave spectrum, we focus on a range of wavenumbers corresponding to 9~15 s waves from the open water dispersion relation. We first determine the apparent attenuation rates of each wavenumber by pairing the wave spectra from different locations. These attenuation rates slightly increase with increasing wavenumber before the FAL and become lower and more uniform against wavenumber in thicker ice after the FAL. The spectral attenuation due to the ice effect is then extracted from the measured apparent attenuation and used to calibrate two viscoelastic wave-in-ice models. For the Wang and Shen (2010) model, the calibrated equivalent shear modulus and viscosity of the pack ice are roughly one order of magnitude greater than that in grease/pancake ice reported in Cheng et al. (2017). These parameters obtained for the extended Fox and Squire model are much greater, as found in Mosig et al. (2015) using data from the Antarctic MIZ. This study shows a promising way of using remote sensing data with large spatial coverage to conduct model calibration for various types of ice cover.

KEY WORDS: pack ice, ocean waves, SAR derived wave spectra, wave attenuation, viscoelastic model calibration

Deleted: gravity wave and model calibration

Deleted: gravity

Deleted: an instance

Deleted: wave propagation in the fall of 2015 in thin…

Deleted: (<0.3 m) and use the resulting attenuation data to calibrate two viscoelastic wave-in-ice models that describe wave evolution. …

Deleted:) in the Beaufort Sea. From Sentinel-1A synthetic aperture radar (SAR) imagery, the ice cover is

Deleted: .

Deleted: retrievals

Deleted: By

Deleted: directional

Deleted: , we obtain wavenumber-dependent

Deleted: , which

Deleted: first appearance of leads

Deleted: that

Deleted: results are

Deleted: through optimization

Deleted: larger than laboratory values

Deleted: areal

Deleted: linear surface gravity wave

1 Introduction

Rapid reduction of Arctic ice in recent decades has become a focal point in climate change discussions (Comiso et al., 2008; Meier and Thomas, 2017; Rosenblum and Eisenman, 2017; Stroeve and Notz, 2018). The reduction emphasizes the need to better understand the complex interaction between the sea ice, the ocean, and the atmosphere. One of these interaction processes is between ocean waves and sea ice. Ocean waves help to shape the formation of new ice covers (Lange et al., 1989; Shen et al., 2001), break existing ice covers (Kohout et al., 2016), modify the upper ocean mixing (Smith et al., 2018), or potentially compress sea ice through wave radiation stress (Stopa et al., 2018a). In turn, ice covers suppress wave-wind interaction by reducing the fetch. They also alter the wave dispersion and attenuation through scattering and dissipation (Squire, 2007, 2018, 2020).

Modeling surface gravity waves in polar oceans requires the knowledge of many source terms. These source terms include wind inputs and dissipation, nonlinear transfer between frequencies, and wave-ice interaction. WAVEWATCH III® (WW3, WAVEWATCH III® Development Group, 2019), one of the most widely used third-generation wind-wave models for global and regional wave forecasts, has implemented several dispersion/dissipation (IC0, IC1, IC2, IC3, IC4, and IC5) and scattering (IS1 and IS2) parameterizations, called "switches" in WW3, to estimate the ice effect on waves. Of the two scattering switches, IS1 redistributes a constant fraction of the incoming wave energy to all directions isotropically. IS2 adopts a linear Boltzmann equation and an estimation of maximum floe diameter due to ice breakup to model wave scattering, combined with a creep related dissipation. As will be discussed in section 3.2, scattering is negligible in the present dataset, hence will not be considered in the present study. Of the six different dispersion/dissipation parameterizations, IC0 and IC1 are out-of-date. IC4 is empirically determined from data obtained in the Southern Ocean. IC2 is based on a theory where wave damping is entirely due to the eddy-viscosity in the water body beneath the ice cover. The other two parameterization, IC3 and IC5 both assume that wave damping is due to the processes within the ice cover alone. In this study, we will focus on IC3 and IC5 parameterizations. The same method may be applied to calibrate IC2. Both IC3 and IC5 theorize that sea ice can store and dissipate mechanical energy, hence they model the ice cover as a viscoelastic material. The storage property is reflected in the potential and elastic energy, and the dissipative property is in the equivalent viscous damping. The difference between IC3 and IC5 is that IC3 is an extension of the viscous ice layer model with a finite thickness (Keller, 1998) by including elasticity into a complex viscosity (Wang and Shen, 2010), while IC5 is an extension of the thin elastic plate model (Fox and Squire, 1994) introduced by Mosig et al. (2015) by adding viscosity into a complex shear modulus (equivalent to the complex viscosity via the Voigt model). Below we will refer to these two viscoelastic models as WS and FS respectively. Each of the two models shows a frequency-dependent wave propagation determined by the dispersion relation. This relation, which depends on the viscoelastic parameters, specifies how the wavenumber $k = k_r + ik_i$ is related to the wave frequency f. The complex wavenumber k contains a real part k_r which determines the wave speed and an imaginary part k_i which determines the damping rate. To use these models for wave forecasts in ice-covered seas, one needs to determine the viscoelastic parameters

Deleted: The rapid

Deleted: . The fact that this reduction exceeds model predictions (Stroeve et al., 2007;

Deleted:)

Deleted: , redistribute wave energy, suppress wave-wind interaction

Deleted: wave breaking

Deleted: To account for

Deleted: effects in wave propagation, the spectral wave model

Deleted:)

Deleted: included

Deleted: (WAVEWATCH III® Development Group, 2019)….

Deleted: Therefore, the energy dissipates and the dispersion changes when waves propagate through an ice field.

Deleted: these equivalent elasticity and equivalent viscosity

for all types of ice covers. To derive these parameters using first principles is challenging, as demonstrated by de Carolis et al. (2005), who obtained the viscosity of grease ice using principles in fluid mechanics of a suspension. Alternatively, an inverse method has been adopted to parameterize IC3. Using in-situ data from the R/V Sikuliaq field experiment (Thomson et al., 2018), the WS model was calibrated to match the observed wavenumber and attenuation (Cheng et al., 2017). This calibration was carried out in a marginal ice zone (MIZ) populated predominantly with grease/pancake ice. Although it showed good agreement between the calibrated model and the field data in the frequency band containing most of the wave energy, these calibrated values are limited to the grease/pancake ice type. Further into the ice cover, where more rigid ice with larger floes is present, how the viscoelastic parameters might change is unknown at present. Note that models can only be as robust as the training data. Therefore, using a broader type of sea ice data will result in a more robust model.

Advancements made in remote sensing technology have provided opportunities for such model calibration. Ardhuin et al. (2017) developed a method to conditionally invert from ice-covered water wave orbital motion to directional wave spectra from the synthetic aperture radar (SAR) images based on the velocity bunching mechanism. The methodology is furthered improved in Ardhuin et al. (2018) and Stopa et al. (2018b) to study wave state in ice-covered Beaufort Sea using SAR images, which were captured in the R/V Sikuliaq field experiment by the satellite Sentinel-1A. Stopa et al. (2018b) retrieved wavenumber-dependent spectra under the partially and fully ice-covered regions by substantially reducing data contamination by ice features with similar length scale as the wavelength. Using the SAR retrieved wave spectra, Stopa et al. (2018b) found that the significant wave height attenuated steeply prior to the first appearance of ice leads (denoted as FAL hereafter), with milder attenuation rate after the FAL. The definition of FAL is described in Appendix A. Furthermore, Monteban et al. (2019) used two overlapping burst images from the Sentinel-1 separated by ~ 2 s to investigated wave dispersion in Barents Sea. Based on the method proposed by Johnsen and Collard (2009), this time separation between subsequent images was sufficient to result in a less noisy and higher quality imaginary spectrum, therefore, allowed them to obtain spatiotemporal information of the dispersion relation. Their results showed that for long waves (100m~350m) in thin ice (<40 cm) the dispersion relation was the same as in open water.

This study uses the dataset reported in Stopa et al. (2018b). It includes two parts of data analysis: obtaining spectral wave attenuation rates from the retrieved wave data, and then use these attenuation rates for wave-in-ice model calibration. This paper is organized as follows: section 2 introduces wave spectra data from Stopa et al. (2018b) used in this study. From this data, we obtain the dominant wavenumbers and the related wave directions over the studied domain. In section 3, we use the directional wave spectra to derive the apparent attenuation rate and then the attenuation rate due to sea ice alone. In section 4, we calibrate two viscoelastic wave-in-ice models using the obtained wavenumber-dependent attenuation data. The methodology presented in these two sections is similar to that in Cheng et a. (2017) with modifications to resolve the difference of wave spectral data types. In Cheng et al. (2017), the spectral data was between energy and frequency, while in Stopa et al. (2018b) it was between energy and wavenumber. Section 5

Deleted: are
Deleted: equivalent
Deleted: the
Deleted: will
Deleted: the wider types
Deleted: that models have been trained
Moved (insertion) [1]
Moved (insertion) [2]
Formatted: Font colour: Auto

discusses the characteristics of wavelength and attenuation in pack ice, calibrated viscoelastic parameters, and wave attenuation modeling. The final conclusions are given in section 6.

2 Data description

During the R/V Sikuliaq experiment, the Sentinel-1A equipped with a synthetic aperture radar (SAR) acquired six sequential images around 16:50 UTC on 12 October 2015. These SAR images covered a 400 km by 1,100 km region including open water, grease/pancake ice, and pack ice (refer to Figure 1 in Stopa et al. (2018b)). A large wave event during this time with wave heights exceeding 4 m in the captured region provided quality wave data. From these SAR images, Stopa et al. (2018b) obtained two-dimensional wave spectra data $E(k_x, k_y)$ for most part of this ice-covered region, where E indicates wave energy density, k_x and k_y are the wavenumber components in the range and azimuth directions of the satellite track, respectively. Details of this dataset and its retrieval may be found in Stopa et al. (2018b). We convert the two-dimensional spectrum at each location into an equivalent wavenumber-direction spectrum $E(k_r, \theta)$, where $k_r = \sqrt{k_x^2 + k_y^2}$ and $\theta = \text{atan}(k_y/k_x)$ indicate wavenumber and direction, respectively. The wavenumber is discretized from 0.011 m^{-1} to 0.045 m^{-1} with an increment of 0.002 m^{-1}, and the direction is discretized into 360 bins with a 1° bin width. We then define wavenumber-dependent main wave directions for each given spectrum, $E(k_r, \theta)$ in the following way. For each wavenumber k_r we fit the corresponding E curve with a Gaussian function, where an example is given in Figure S1 of the supplemental material. The mean of this Gaussian function is defined as the main wave direction θ_{k_r} for this k_r. Furthermore, we define the dominant wavenumber, $k_{r,dominant}$, to be the one corresponding to the maximum directionally integrated wave energy $\int E(k_r, \theta) d\theta$.

An overview of the processed wave conditions in terms of the dominant wavenumber and its main direction is given in Figure 1(a), along with the locations of the ice edge and other in-situ observations. The associated ice conditions in the region are presented in Figures 1(b)(c). Significant spatial variability is observed in both the wave and ice conditions. Figure 1(a) presents a subregion captured by the SAR images covering from a portion of Alaska to the last azimuth position where waves are detectable in the images. Colors indicate the dominant wavenumber distribution of the retrievals, and arrows indicate their main directions. Cell size is coarsened to 12.5 km × 12.5 km to enhance visualization. The ice edge is indicated by the contours of ice concentration (<0.4) from AMSR2 (Advanced Microwave Scanning Radiometer 2, http://doi.org/10.5067/AMSR2/A2_SI12_NRT). An in-situ buoy: AWAC-I (a subsurface Nortek Acoustic Wave and Current buoy, moored at 150°W, 75°N) is marked by a magenta asterisk. Except for the in-situ observations from the Sikuliaq ship (green diamond) and several drifting buoys (blue dots) near the ice edge, ice morphology information including ice types and their partial concentrations are absent. Nevertheless, the FAL (red dots) presumably marks the separation between discrete floes and a semi-continuous ice cover with dispersed leads. The ice condition below (before) the FAL was more complex with thinner ice and lower concentration than that above (after) the FAL.

Moved up [1]: Ardhuin et al.

Moved (insertion) [3]

Deleted: (2017) developed a method to invert from wave orbital motion to directional wave spectra from SAR images of waves in sea ice based on the velocity bunching mechanism. Stopa et al. (2018b) refined this methodology for the partially and fully ice-covered regions by substantially reducing data contaminated by ice features with similar length scale as the wavelength. Using SAR retrieved wave spectra, the authors found the significant wave height attenuated steeply prior to the first appearance of ice leads (denoted as FAL hereafter), with milder attenuation rate after the FAL. …

Deleted: ice and

Deleted: condition

Deleted: available

Deleted: studied

Deleted: is

Deleted: Figure 1. More details of the retrievals are given in Stopa et al. (2018b

Deleted: largest

Deleted: last observed visually

Formatted: Font: Bold

Deleted: the dominant wave direction defined in section 2.

Deleted: black

Deleted: black

Deleted: “

Deleted: ”

Deleted: of a subregion

Deleted: Based on the distribution of SAR retrievals, we…

We select the study domain defined by the azimuth from 450 to 750 km and the range from 0 to 400 km. This domain contains most of the wave data retrieved in the pack ice field. Figures 1(b)(c) show the distributions of ice concentration from AMSR2 and ice thickness from SMOS (Soil Moisture and Ocean Salinity, https://icdc.cen.uni-hamburg.de/1/daten/cryo-sphere/l3c-smos-sit.html), respectively, in the region of interest. As shown in Cheng et al. (2017) (Supporting information Figures S6 and S7), these two ice products compared the best with in-situ observations in the MIZ. Their accuracies in the pack ice zone are uncertain. The purpose of this work is to retrieve the spectral wave attenuation and use the result to calibrate viscoelastic models in regions dominated by thin pack ice (thickness<0.3 m). As shown in Figure 1(a), $k_{r,dominant}$ generally declines crossing the FAL towards the north. Before the FAL, $k_{r,dominant}$ increases in the direction of increasing range and decreasing ice concentration but is insensitive to ice thickness variation. After the FAL, $k_{r,dominant}$ decreases in the wave propagating direction (arrows) associated with the increase of ice thickness, where the ice field is presumably a semi-continuous cover populated with leads.

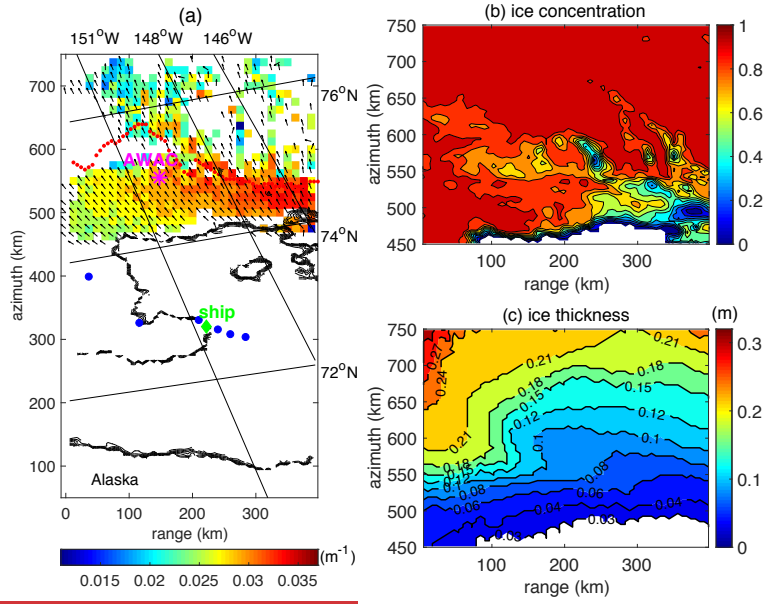

Figure 1. (a) Overview of the retrieved data distribution around 16:50 UTC on 12 October 2015. Colors represent the dominant wavenumber and arrows represent the main direction of the dominant wavenumber. Red dots indicate the first appearance of leads (FAL). Locations of the Sikuliaq ship and the buoys operating at that time are indicated by green diamond and blue dots, respectively. AWAC-I is marked by a magenta asterisk. Ice edges are indicated by contours of ice concentration < 0.4 from AMSR2 (b)(c) Distributions of ice concentration (AMSR2) and ice thickness (SMOS) in the selected region, respectively.

$d\theta$Figures 2(a)(b) show two-dimensional histograms of the main wave direction for each wavenumber θ_{kr} before and after the FAL, respectively, where wave direction is defined in the meteorological convention (i.e. the direction 'from' in degrees clockwise from True North). Grayscale indicates the occurrence frequency of

Moved (insertion) [4]

Deleted: This work is to retrieve wave attenuation and use the result to calibrate viscoelastic models in thin pack ice (<0.3 m) dominant region.

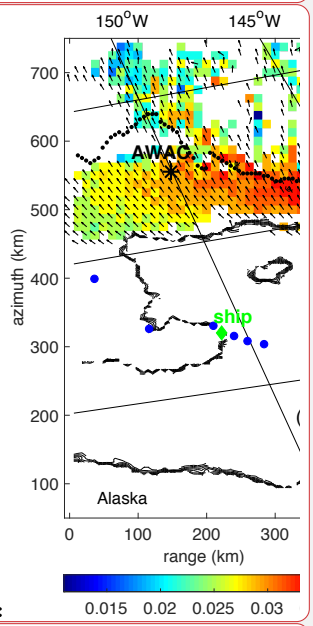

Deleted:

Deleted: wave directions. Black

Deleted: black

Deleted: This paper is organized as follows: site description and wave characteristics are depicted in section 2. We use the directional wave spectra retrieved from the Sentinel-1A SAR imagery to derive the wavenumber-dependent attenuation in section 3. The methodology of model calibration and results are presented in section 4. The methodology of calibrating IC3 used in Cheng et al. (2017) based on wave energy spectrum $E(f,\theta)$ in terms of frequency f needs to be modified for the present wavenumber-based spectra. Section 5 discusses the characteristics of ... [1]

Moved up [3]: $d\theta$.

Moved up [4]: generally declines crossing the FAL towards the north. Before the FAL, $k_{r,dominant}$

Deleted: varies with ice concentration but is insensitive to ice thickness variation and wave directions. After the FAL, $k_{r,dominant}$ decreases in the wave propagating direction associated with the increase of ice thickness.[2]

Formatted: Font colour: Text 1

θ_{k_r} in each k_r bin. We observe a significant change of θ_{k_r} crossing the FAL: θ_{k_r} before the FAL spreads from 160° to 190°, while θ_{k_r} is more tightly clustered from 180° to 200° after the FAL. The difference before and after the FAL is most significant for $k_r < 0.035$ m^{-1}

For the subsequent spectral analysis, we further restrict k_r to 0.019 m$^{-1} \leq k_r \leq \min(2\pi/\lambda_c, 0.045\text{m}^{-1})$, where λ_c is the azimuth cutoff indicating the minimum resolvable wavelength from the SAR imagery (Stopa et al., 2015; Ardhuin et al., 2017). Below this wavelength, the patterns of ice-covered ocean surface roughness from SAR imagery are more related to ice features rather than waves (Stopa et al., 2018b). For $k_r < 0.019$ m^{-1}, energy density $E(k_r, \theta_{k_r})$ is small with high spatial variation (Figure B1 in Appendix B), hence treated as noise band and removed from further study.

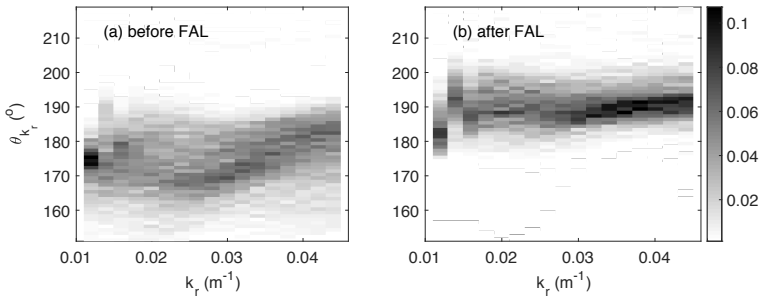

Figure 2. Two-dimensional histogram of θ_{k_r} and k_r collected (a) before and (b) after the FAL. Grayscale represents the occurrence frequency of θ_{k_r} in each k_r bin.

The corresponding frequency f (wave period T) range is estimated as 0.067 to 0.11 Hz (9 to 15 s) using the open water dispersion relation, $(2\pi f)^2 = g k_{ow}$, where g is the gravitational acceleration, k_{ow} indicates the wavenumber in open water. The actual dispersion relation which is likely dependent on the ice condition cannot be measured from our instantaneous SAR data. Using accelerometers deployed on ice floes (Fox and Haskell, 2001) and from marine radar or buoy data (Collins et al., 2018), it was found that the wavenumber in ice-covered region within about 10 km from the ice edge was close to that in open water. Further into the ice cover, Monteban et al. (2019) used two overlapping burst images from the Sentinel-1 separated by ~ 2 s to investigated wave dispersion in the Barents Sea. The ice concentration and thickness in their study were similar to the present study. The computed wave dispersion within the sea ice for long waves (peak wavelengths > 100 m) was in good agreement with the open-water dispersion relation.

3 Wave attenuation

In this section, we first obtain the apparent spectral wave attenuation by pairing the directional spectra at different locations. We then remove the contributions of wave energy between pairs of locations from wind input, wave breaking dissipation, and nonlinear transfer between frequency components to extract the spectral

Deleted: $2\pi/\lambda_c$,
Deleted: A1
Deleted: the
Formatted: English (US)
Deleted: i.e.,
Deleted: Note the
Deleted: range of frequencies in the present case might be different due to the possible change of …
Deleted: in pack
Deleted: . The dispersion relation
Deleted: the
Deleted: cover
Deleted: near
Deleted: open sea (≲10 km)
Formatted: English (UK)
Deleted: Deriving
Formatted: Normal
Formatted: English (UK)

attenuation due to ice effects alone. These spectral attenuation rates due to ice will be used in section 4 to calibrate two viscoelastic wave-in-ice models.

3.1 Apparent wave attenuation

We define an apparent wave attenuation for each k_r by assuming exponential decay of the wave spectral densities from location A to location B:

$$\alpha(k_r) = \frac{1}{2Dcos(|\bar{\theta}-\theta_{AB}|)} ln\left(\frac{E_A(k_r,\bar{\theta})}{E_B(k_r,\bar{\theta})}\right) \quad (1)$$

where $\bar{\theta} = \frac{\theta_{k_r,A}+\theta_{k_r,B}}{2}$ is the average of the main wave directions at A and B; D and θ_{AB} are the distance and direction from A to B in the longitude-latitude coordinates, respectively. A selected pair of A and B is named as a pair hereafter. To reduce the uncertainties of naturally present ice and wave variability, a set of quality control criteria are applied to a pair before further analysis:

1) Ignore substantially oblique waves. The difference between $\bar{\theta}$ and the vector from location A to location B is restricted to $|\bar{\theta} - \theta_{AB}| \leq 15°$.
2) Avoid strong spatial variations of ice condition between A and B. Distance between A and B is restricted to $D \leq 60$ km.
3) As the wave state changes significantly across the FAL as mentioned in section 2, no pair across the FAL is selected. This criterion enables us to detect, if any, the influence of ice morphology on wave attenuation.
4) Ensure point A and B are both subject to the same wave system, the Pearson correlation coefficient between energy spectra $E_A(k_r,\theta)$ and $E_B(k_r,\theta)$ is required to be greater than 0.9. The Pearson correlation coefficient is defined as $r = \frac{\Sigma_i(x_i-\bar{x})(y_i-\bar{y})}{\sqrt{\Sigma_i(x_i-\bar{x})^2}\sqrt{\Sigma_i(y_i-\bar{y})^2}}$, where x_i and y_i are the PSD values at the i^{th} wavenumber.
5) Exclude outliers of the spectral attenuation where wave energy of B is higher or close to that of A. Thus, $\alpha(k_r) > 10^{-6}$ m^{-1} is required.
6) A selected pair has at least 10 data points of $\alpha(k_r)$ to do calibration in section 4.

We obtain 2634 pairs (2194 pairs before the FAL, and 440 pairs after the FAL) through the above criteria to calculate the apparent wave attenuation $\alpha(k_r)$ by Eq. (1). The results are sorted statistically to show the occurrence frequency of $\alpha(k_r)$. The α domain is equally divided into 30 bins from 10^{-6} to 10^{-4} m^{-1} in log scale, and the k_r domain is equally divided from 0.011 m^{-1} to 0.0045 m^{-1} with an increment of 0.002 m^{-1} as mentioned earlier. Figures 3(a)(b) show two-dimensional histograms of α against k_r before and after the FAL, respectively. Grayscales represent the occurrence of α at each combined bin of α and k_r. Red curves indicate the most frequent occurrence of $\alpha(k_r)$ against k_r. It is observed that more data are obtained before the FAL, with a slightly increasing trend of $\alpha(k_r)$ versus k_r before the FAL, while $\alpha(k_r)$ obtained after the FAL are mostly lower and independent of k_r.

The range of this apparent spectral attenuation is in agreement with Stopa et al. (2018b), in which, the authors selected multiple tracks throughout the ice region and focused on the overall decay of the significant wave height over hundreds of kilometers. The reduction of attenuation crossing the FAL shown in Figure 3 is also consistent with Stopa et al. (2018b), who reported a drop of attenuation of the significant wave height after the FAL. In Appendix B, we show the results of this long-range attenuation against wavenumber. (Figure

Deleted: ice
Formatted: English (UK)
Deleted: an
Deleted: Difference
Formatted: Font: Italic
Formatted: Font: Italic
Formatted: Font: Italic
Formatted: Font: Italic
Deleted: change rapidly
Deleted: , in order
Deleted: compare
Deleted: the
Deleted: The
Deleted: Similarity of wave spectra patterns indicates that the wave fields from A to B
Deleted: dominated by
Deleted: same wave system.
Formatted: Font: Italic
Deleted: The empirical thresholds of criteria 2) and 4) are determined based on the sensitivity of the number of selected pairs depending on these values. Figure
Deleted: , where the α domain is divided into equal 30 bins in log scale from 10^{-6} to 10-4 m^{-1} ….
Deleted: collected
Deleted: and
Deleted: slight
Deleted: the

B1). The difference of attenuation obtained by the two methods, one based on short distances (<60 km) to reduce the effect of ice type variability and the other over long distances (~300 km) is discussed in section 5.

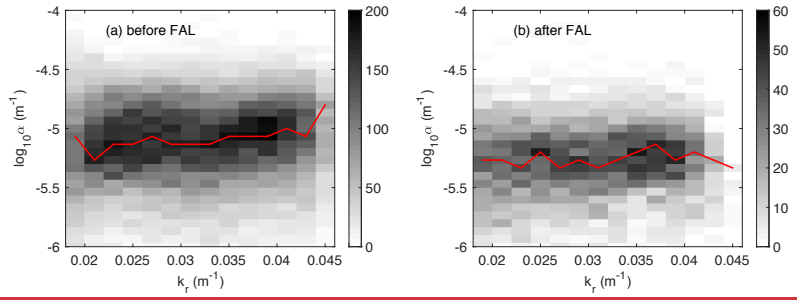

Figure 3. Smoothed two-dimensional histograms of wavenumber k_r and the apparent attenuation α, (a) before the FAL and (b) after the FAL. The α domain is equally divided into 30 bins in the log scale from 10^{-6} to 10^{-4} m^{-1}. The k_r domain is divided from 0.011 m^{-1} to 0.0045 m^{-1} with an increment of 0.002 m^{-1}. Grayscale indicates the occurrence of α in each α-k_r bin from the selected pairs. The red curve indicates the highest occurrence of α against k_r.

Because of the large study domain and the apparent difference of $k_{r,dominant}$ in the east-west direction before FAL as shown in Figure 1(a), it is worthwhile examining the regional variability. Figure 4 displays the results related to α and k_r in three subdomains from west to east bounded by longitudes: (150°W, 151°W), (148°W, 149°W) and (146°W, 147°W). The left column shows 467, 233 and 132 pairs selected in the three longitude bins, respectively. Each segment indicates a pair selected in section 3.1, with ends corresponding to the locations A, B and its color indicates the mean ice thickness between the two. In the middle column, the α values corresponding to $k_r = 0.019$, 0.025, 0.031 and 0.039 m^{-1} obtained from these pairs are separated into two groups: before and after the FAL. In each subdomain delineated by the longitude and the FAL, the distribution of α for each k_r is presented by a violin plot, whose width indicates the probability density distribution of α and a circle marker inside indicates the median. These violin plots show that α before the FAL is larger than that after the FAL for all k_r in all three subdomains. We note that the sample size after the FAL in the eastern-most subdomain (146°W, 147°W) is the lowest, corresponding to the largest variability of the violin plots. To track wave spectrum evolution from nearer the ice edge towards the interior ice zone, we collect wave power spectral densities (PSDs, $\int E(k_r,\theta)d\theta$) at the north end of each selected pairs in the left column. The averaged PSDs of this collection per 0.1 degree in latitudes are presented by curves in the right column, where colors indicate the latitude. As defined earlier, k_r associated with the peak of a PSD curve is $k_{r,dominant}$. Before the FAL the magnitude of PSD drops rapidly while $k_{r,dominant}$ varies slightly as the latitude increases. In contrast, the PSDs change slowly after the FAL while $k_{r,dominant}$ decreases quickly. Note that at high latitudes, PSD at $k_{r,dominant}$(red) is higher than that of the same wavenumber at low latitudes. We will revisit this phenomenon in the discussion section.

Deleted: A1
Deleted: distance
Deleted: distance
Moved (insertion) [5]
Moved (insertion) [6]
Deleted: correspond
Deleted: are
Deleted: and
Formatted: Font colour: Text 1
Deleted: In
Formatted: Font colour: Text 1
Deleted: right column,
Formatted: Font colour: Text 1
Formatted: Font colour: Text 1
Deleted:) retrieved
Formatted: Font colour: Text 1
Deleted: locations
Formatted: Font colour: Text 1
Deleted: the ends of the
Formatted: Font colour: Text 1
Deleted: are given. Curves indicate the
Formatted: Font colour: Text 1
Deleted: PSD
Formatted: Font colour: Text 1
Deleted: , with latitude marked
Formatted: Font colour: Text 1
Formatted: Font colour: Text 1
Formatted: Font colour: Text 1
Deleted: increase of
Deleted: varies

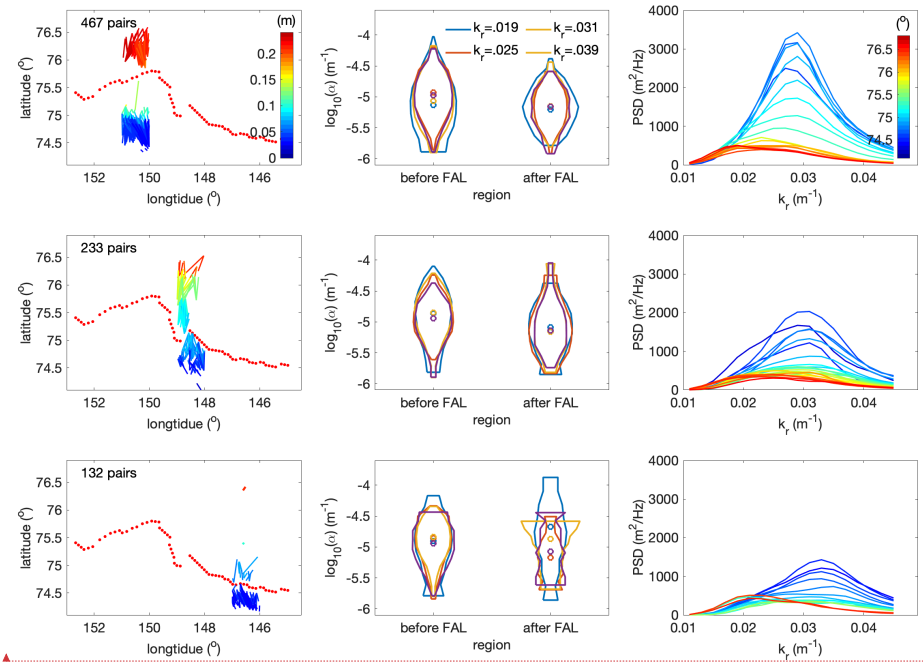

Figure 4. Close view in three selected longitude intervals: (150°W, 151°W), (148°W, 149°W) and (146°W, 147°W). (Left column) Geographical distribution of the selected pairs, each of which is represented by a segment with color indicating the mean ice thickness. Red dots represent the FAL. (Middle column) Violin plots of the relevant α grouped by wavenumbers and before/after the FAL. (Right column) Evolution of the PSD of wave spectra per 0.1° in latitude. Note that in the rightmost interval (bottom row) the red PSD curves correspond to the few very short red segments near 76.5°N.

3.2 Wave attenuation due to ice effect

Following Eq. (1), the apparent attenuation obtained above is determined by the energy difference between two locations. This apparent attenuation is the result of multiple source terms, including the wind input S_{in}, damping through wave breaking and swell dissipation S_{ds}, the energy transfer due to nonlinear interactions among spectral components S_{nl}, and the dissipation/scattering of wave energy due to ice cover S_{ice}. In this section, we derive the attenuation rate due to S_{ice} from the measured apparent attenuation α.

The radiative transfer equation for surface waves concerning all the above effects is

$$\frac{\partial E}{\partial t} + \frac{\partial (c_g + U)E}{\partial x} = (1 - C)(S_{in} + S_{ds}) + S_{nl} + CS_{ice} \quad (2)$$

where $E = E(k_r, \theta, x, t)$ is the power spectral density depending on wavenumber, direction and location x; c_g is the group velocity; U is the current velocity. Note that U in this region is below 0.1 m/s, according to OSCAR (Ocean Surface Current Analyses Real-time, https://www.esr.org/research/oscar/). Because the current speed is at least one order of magnitude below the estimated c_g using the open water dispersion relation, we may drop it from Eq. (2). Furthermore, consistent with the fact that the dispersion relation in this

Formatted: English (US)

Deleted: Geological

Deleted: SAR retrieved

Deleted: in the subdomain.

Deleted: the dissipation

Deleted: (k_r, θ, x)

Deleted: by assuming

study is close to that of the open water, c_g is relatively constant. Adopting the exponential wave decay along x, i.e., $E(k_r, \theta, x) = E(k_r, \theta, x = 0)e^{-2\alpha x}$, we have $\frac{\partial (c_g + U)E}{\partial x} \approx c_g \frac{\partial E}{\partial x} = -2c_g \alpha E$.

Next, we examine the temporal derivative of wave energy $\frac{\partial E}{\partial t}$. It is challenging to calculate $\frac{\partial E}{\partial t}$ from the nearly instantaneous SAR imagery. Instead, we estimate $\frac{\partial E}{\partial t}$ using hourly wave spectra data from two sources around the time stamp of the SAR imagery: the in-situ AWAC-I marked in Figure 1 and the WW3 simulations of the whole domain (REF run of Ardhuin et al., 2018). From the AWAC-I data, we obtain $\frac{\partial E}{\partial t}$ and compare that with $c_g \frac{\partial E}{\partial x}$ using SAR retrieved wave data at the AWAC-I site. From the WW3 simulations, we obtain both terms over the whole study domain. Both results consistently show that $\frac{\partial E}{\partial t}$ is at least two orders of magnitude below $c_g \frac{\partial E}{\partial x}$. Thus, $\frac{\partial E}{\partial t}$ is dropped from Eq. (2).

The other source terms S_{in} and S_{ds} are estimated using formulations from Snyder et al. (1981) and Komen et al. (1984). For S_{nl}, we select the Discrete Interaction Approximation (DIA, Hasselmann et al., 1985a, b) to estimate its value. Note that those parameterizations were formulated from open water study. How they might change in the presence of ice covers is an open question. The formulations and associated coefficients used here are described in Cheng et al. (2017). Wherever needed in these formulations, f is approximated by the open water dispersion relation with the measured k_r. Ice concentration is from AMSR2, ice thickness is from SMOS, and wind data is from the Climate Forecast System Reanalysis (CFSR, Saha et al., 2010).

Ice-induced wave attenuation is known from the dissipation of wave energy and scattering of waves (e.g., Wadhams et al., 1988; Squire et al., 1995; Montiel et al., 2018). Here we attribute the attenuation entirely to the dissipative process with the following arguments. Ardhuin et al. (2018) reported that in the studied region, ice floe scattering is a weaker effect on wave attenuation compared with other processes, including the boundary layer beneath the ice, inelastic flexing of ice cover, and wave-induced ice fracture. The inelastic flexing and ice fracture may be considered as part of the dissipative mechanism within the ice cover already included in the viscous coefficient, but scattering is a re-distribution of energy, which must be isolated from the apparent attenuation before using the data to calibrate the viscoelastic models. We estimate the scattering effect based on the study of Bennetts and Squire (2012) as follows. In that study, wave attenuation by floes, cracks and pressure ridges were examined. In the absence of in-situ observations, we assume that few and small ridges are present in the studied ice cover (thickness < 0.3 m), hence the effect of ridges is negligible. In our case of long waves propagating through such thin ice cover, Bennetts and Squire (2012) have shown that the floes produce much more attenuation than the cracks. Without in-situ observation, WW3 simulations (REF run in Ardhuin et al., 2018) implementing wave-induced fracturing of ice floes gave a range of estimated maximum floe diameter from 70 to 150 m. Using this range of floe diameter, the theoretical scattering results from Bennetts and Squire (2012) indicate that the floe scattering-induced attenuation is about 10^{-7} m^{-1}, which is negligible compared to the α shown in Figure 3.

With all the above simplifications and the assumed exponential decay of wave energy, Eq. (2) becomes:

$$-c_g 2\alpha E = (1 - C)(S_{in} + S_{ds}) + S_{nl} - C2c_g k_i E \quad (3)$$

Deleted: to be

Deleted: along x and adopting

Deleted: (

Deleted: simulation

Deleted: simulation

Deleted: These

Deleted: (< 25 cm

Deleted: gives

Deleted: k_i^m

which yields

$$k_i = \frac{2c_g\alpha E+(1-C)(S_{in}+S_{ds})+S_{nl}}{2Cc_gE} \quad (4)$$

where k_i is the attenuation rate due to the ice cover. The occurrence of the k_i data is presented by two-dimensional histograms of k_i against k_r in Figure 5. Not surprisingly, since wind effect is low due to the low open water fraction in the study region, and the relatively short distances between the pairs for the nonlinear transfer of energy to accumulate, we observe that k_i is very close to the apparent attenuation α. We will discuss further this ice-induced dissipation in section 5.

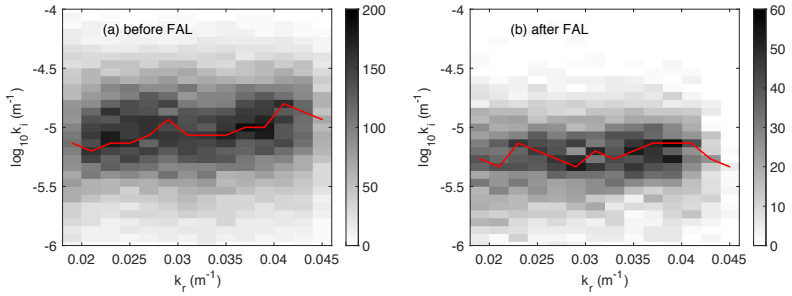

Figure 5. Smoothed two-dimensional histograms of the ice-induced attenuation rate k_i against wavenumber k_r, (a) before the FAL and (b) after the FAL. The attenuation domain is equally divided into 30 bins in the log scale from 10^{-6} to 10^{-4} m^{-1}. Grayscale indicates the occurrence of k_i in each k_i-k_r bin from the selected pairs. The red curve indicates the highest occurrence of k_i against k_r.

4 Wave-in-ice model calibration

In this section, we present the calibration of the WS model and the FS model. We will begin with a brief introduction of the two models then describe the calibration procedure. In both models, k_r and k_i are solved from the respective dispersion relations for given ice thickness and viscoelastic parameters. The viscoelastic parameters are optimized by minimizing the overall difference of $k_i - k_r$ relationship between the models and data obtained in section 3.

4.1 Dispersion relation

The dispersion relations of the two models are written as

$$\sigma^2 - Qgk\tanh kH = 0 \quad (5a)$$

For the WS model,

$$Q = 1 + \frac{\rho_{ice}}{\rho_{water}}\frac{(g^2k^2-N^4-16k^6a^2v_e^4)S_kS_a-8k^3av_e^2N^2(C_kC_a-1)}{gk(4k^3av_e^2S_kC_a+N^2S_aC_k-gkS_kS_a)} \quad (5b)$$

For the FS model,

$$Q = \frac{G_vh^3}{6\rho_{water}g}(1+\mathrm{V})k^4 - \frac{\rho_{ice}h\sigma^2}{\rho_{water}g} + 1 \quad (5c)$$

Deleted: k_i^m

Deleted: k_i^m

Deleted: Figure 5 shows

Deleted: α

Deleted: before and after the FAL, as

Deleted: 3

Deleted: k_i^m

Deleted: , and

Deleted: be

Deleted: discussed

Deleted: the discussion

Deleted: 3

Deleted: and apparent attenuation α,

Deleted: α

Deleted: equal

Deleted: indicate

Moved up [5]: the occurrence of α in each α-k_r bin from the selected pairs. The red

Moved up [6]: The red curve indicates the highest occurrence of α against k_r.¶

Deleted: , k_i

Deleted: with a

Deleted: properties. An optimization procedure is introduced to select the

Deleted: that minimize the

Deleted: model k_i

Deleted: the k_i^m

Deleted: from the SAR over the entire range of k_r.

Deleted: $\frac{(g^2k^2-N^4-16k^6\alpha^2v_e^4)S_kS_\alpha-8k^3\alpha v_e^2N^2(C_kC_\alpha-}{gk(4k^3\alpha v_e^2S_kC_\alpha+N^2S_\alpha C_k-gkS_kS_\alpha)}$

where H is water depth, $\sigma = 2\pi f$ is the angular frequency, ρ_{ice} and ρ_{water} are the densities of ice and water, respectively, $k = k_r + ik_i$ is a complex wavenumber, h is the ice thickness, $a^2 = k^2 - \frac{i\sigma}{\nu_e}$, $S_k = \sinh kh$, $S_a = \sinh ah$, $C_k = \cosh kh$, $C_a = \cosh ah$, $N = \sigma + 2ik^2\nu_e$, $G_\nu = G - i\sigma\nu\rho_{ice}$ and $\nu_e = \nu + \frac{iG}{\rho_{ice}\sigma}$, V is the Poisson's ratio. Equivalent shear modulus G and kinematic viscosity ν in both models are to be calibrated. In this study, we use H = 1000 m for deep water, ρ_{water} = 1025 kg/m^3, ρ_{ice}= 922.5 kg/m^3 and V = 0.3 for ice.

Hereafter, we use superscripts t for the theoretical values and m for the measured data. Specifically, the theoretical wavenumber and attenuation rate are denoted as k_r^t and k_i^t. They are calculated for each set of G, ν values. Attenuation data due to the ice effect obtained in section 3 is denoted as k_i^m. The corresponding wavenumber k_r^m is the discretized k_r values from 0.011 m^{-1} to 0.0045 m^{-1} with an increment of 0.002 m^{-1}.

4.2 Calibration methodology

In this section, we optimize G, ν by fitting $k_i - k_r$ relationship from the model via Eq. (5) to the measured values from Eq. (4). Specifically, for given G and ν, we solve arrays of k_r^t and k_i^t through Eq. (5) for each f densely sampled from 0.0001 Hz to 1 Hz. We then interpolate the results to obtain the theoretical k_i at each wavenumber k_r^m from the data in section 3.2. For each of these k_r^m we have the measured dissipation rate k_i^m shown in section 3.2. We now use an optimization procedure to determine the best-fit parameters G and ν. The objective function for the optimization is defined as the weighted sum of the differences between k_i^t and k_i^m over k_r^m, i.e.,

$$F = \min_{G,\nu} \left\| w(k_r^m)\left(k_i^m(k_r^m) - k_i^t(k_r^m)\right) \right\|_2 \quad (6)$$

where $\|\cdot\|_2$ is the L-2 norm operator, $w(k_r^m)$ is a weighting factor to account for the distributions of wave energy and attenuation rate. Cheng et al. (2017) tested two weighting factors: $w = \int E(\theta, f)d\theta$ and $\int E(\theta, f)f^4 d\theta$ in calibrating the WS model. In that study, the measured data had a range of f varied from 0.05 to 0.5 Hz, and the attenuation rate varied from 10^{-6} to 10^{-3} m^2/s. The authors found that using $w = \int E(\theta, f)d\theta$ fitted attenuation best at the most energetic wave band, while $w = \int E(\theta, f)f^4 d\theta$ performed better to capture significant increasing of k_i at high frequencies. No weighting factor could produce a fitting over the entire spectral attenuation curve. For the present study, the variation of spectral attenuation is small as shown in Figure 5 with no particular region of emphasis, we thus choose $w = \sqrt{\int E(\theta, k_r)d\theta}$ which has a broad band around the peak energy of the wave field.

We choose a search domain (10^{-7} Pa $\leq G \leq 10^{10}$ Pa and 10^{-4} m^2/s $\leq \nu \leq 10^4$ m^2/s) for the WS model. This search domain covers all other reported viscoelastic values for ice covers (e.g., Newyear and Martin, 1999; Doble et al., 2015; Zhao and Shen, 2015; Rabault et al., 2017). For the FS model, it is known that very large G, ν are needed to obtain the level of k_i observed (Mosig et al., 2015). We thus choose a large search domain 10 Pa $\leq G \leq 10^{20}$ Pa and $10 \leq \nu \leq 10^{15}$ m^2/s. This parameter range is far beyond the measured data from

Deleted: $S_\alpha = \sinh\alpha h$

Deleted: $C_\alpha = \cosh\alpha h$, h is the ice thickness, $\alpha^2 = k^2 - \frac{i\sigma}{\nu_e}$,

Deleted: For each pair selected in

Deleted: 3

Deleted: modelled

Deleted: k_i^m over the k_r^m domain. Note that k_i, k_r in the models are solved simultaneously for an array of f. We need to convert the theoretical k_i-f relation to k_i-k_r^m.

Deleted: k_r

Deleted: k_i

Deleted: , and

Deleted: k_r^m.

Deleted: k_i

Deleted: $\|w(k_r^m)(k_i^m - k_i)\|_2$

Deleted: using

Deleted: component

Formatted: Font: Times New Roman

solid ice (Weeks and Assur, 1967). The global optimization procedure is performed by using the genetic algorithm with function *ga* in MATLAB and Global Optimization Algorithm Toolbox (R2016a).

4.3 Results

For the WS model, the optimized G, ν are gathered into a small cluster around $G \cong 10^{-4}$ Pa and a large cluster around $G \cong 10^{5}$ Pa with large variation in ν. The existence of two separate clusters of calibrated results was also found in grease/pancake mixtures near the ice edge (Cheng et al., 2017). Note that multiple solutions (optimized G, ν pairs) could be obtained in optimizing a nonlinear system such as shown in Eq. (5). Thus, constraints are applied to select solutions that are physically plausible. Note that the solutions around $G = 10^{-4}$ Pa, and solutions with ν near 10^4 m^2/s lead to the residual from Eq. (6) insensitive to G. It implies that the modeled material is viscous dominant with almost nil elastic effect. Those cases are incompatible with the pack ice condition, thus removed in the following analysis. Scatter plots of the remaining data points (G, ν) are presented by Figure S2 in the supplemental material. For these remaining data, we apply the bivariate Gaussian distribution to obtain the 90% probability range of (G, ν) before and after the FAL, respectively. Means and covariances of the related probability density functions are given in Table 1. A slight difference of distributions of G, ν before and after the FAL is noticed. The mean of elasticity (viscosity) is slightly lower (higher) before the FAL than that after the FAL. The results imply that the ice layer behaves more elastic in the inner ice field and more viscous towards the ice edge. It is worth noting that the ranges of both G and ν are about one order of magnitude greater than those of the grease/pancake ice (Cheng et al., 2017). As expected, the effective elasticity in the WS model for more solid ice is closer to the elastic modulus of sea ice.

Table 1. Statistical features of the clusters of G and ν from the WS model and FS model calibration. The mean (μ) and covariance (cov) of $X = \log_{10} G$ and $Y = \log_{10} \nu$

	μ_X	μ_Y	$cov(X,X)$	$cov(X,Y)$	$cov(Y,Y)$
WS Model					
Before FAL	5.07	1.51	0.07	0.07	0.81
After FAL	5.25	1.32	0.11	0.27	1.26
FS Model					
Before FAL	17.39	10.82	2.83	1.42	1.00
After FAL	16.26	9.51	1.90	0.95	0.75

For the FS model, the calibrated (G, ν) are clustered, where scatter plots of (G, ν) are given in Figure S3 in the supplemental material. Hence all data points are used in the bivariate Gaussian fitting. The resulting mean and covariance values are also given in Table 1. Notice that the mean values of G, ν from the FS model are extremely larger than the intrinsic values of ice. The distribution of calibrated values is further discussed in the discussion section.

Deleted: using

Deleted: As

Deleted: solving optimal problem of the

Deleted:),

Deleted: physical. In the optimization, we reject the …

Deleted: that

Deleted: is

Deleted: Because both situations imply

Deleted: model becomes

Deleted: , inconsistent

Deleted: the physical behaviors of

Deleted: Furthermore

Deleted: to the rest of points

Deleted: Slight

Deleted: slight

Deleted: Scatter plots of (G, ν) are given in Figure S3 in the supplemental material.

Hereafter we only elaborate on the results of the WS model. Figures 6(a) shows the overall comparison of $k_i - k_r$ between the measurements (gray) and the WS model (black). Both the median (solid curve) and 90% boundaries (dash curves) are in good agreement. In Figure 6(a), we superimpose an empirical model from Meylan et al. (2014), which is also included in WW3 to account for the ice effect as switch IC4. By fitting the wave buoy data from the Antarctic MIZ obtained in 2012, Meylan et al. (2014) proposed a simple period-dependent attenuation rate $k_i(T) = \frac{2.12\times10^{-3}}{T^2} + \frac{4.59\times10^{-2}}{T^4}$, which is converted into a $k_i - k_r$ relation through the open water dispersion relation. The empirical formula predicted that attenuation was consistent with the range we obtained here, but with a higher sensitivity to k_r. Figure 6(b) shows the normalized wavenumber $\frac{k_r}{k_{ow}}$ against f using the optimized G, ν in the WS model. The deviation of $\frac{k_r}{k_{ow}}$ from 1 is less than 5%, indicating the modeled wave dispersion agrees with the open water dispersion relation. It is consistent with Monteban et al. (2019) who investigated wave dispersion in ice from the SAR data in the Barents Sea, as the studied range of wavelength and ice thickness are similar. The counterpart of the FS model is given Figure S4 in the supplemental material.

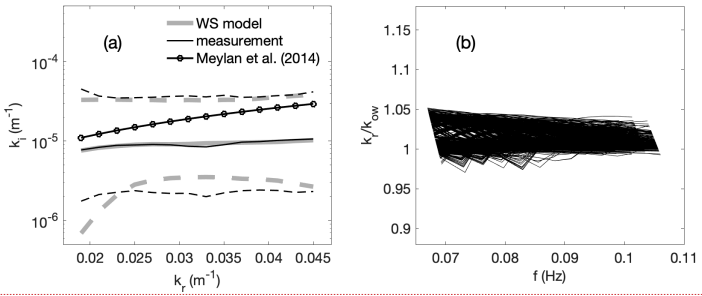

Figure 6. (a) Comparison of ice-induced attenuation k_i between measured data from Eq. (4) and the WS model predictions; Solid lines are mean values and dashed lines are 90% confidence intervals. Gray-thick lines are the calibrated WS model and black thin lines from the data. Black line with symbol is the empirical model from Meylan et al. (2014); (b) the corresponding k_r/k_{ow} from the calibrated WS model against wave frequency.

Figures 7(a)(b) show distributions of calibrated G and ν from the WS model in the azimuth-range domain, respectively. Contours represent ice thickness distribution from SMOS. The FAL is marked as red dots. The spatial domain is divided into 12.5 km × 12.5 km cells to enhance visualization. Cell color indicates the averaged value of $\log_{10}G$ and $\log_{10}\nu$ of all pairs with midpoints inside the cell. Ignoring the outliers, Figure 7(a) shows that G is generally larger after the FAL (thicker ice with leads) than before the FAL, while ν has an opposite trend. Note that the outliers could be from multiple sources, such as noise in the retrieved wave data, spatial variability of ice condition, assumptions made in selecting pairs and calculating attenuation, and the adopted genetic algorithm in the model calibration. The counterpart of the FS model is given in Figure S5 in the supplemental material.

Deleted: -k_r
Deleted: Gray
Deleted: k_i-k_r
Deleted: %.
Formatted: English (UK)
Formatted: English (US)
Deleted: results
Deleted: it
Deleted: as well as

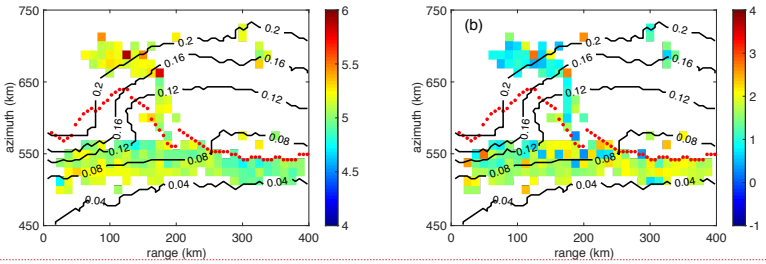

Figure 7. (a) Distribution of $\log_{10}G$ in averaged 12.5 km×12.5 km grid in the range-azimuth plane. Cell color indicates the averaged $\log_{10} G$ of all pairs with midpoints inside a cell; Contours indicate SMOS ice thickness; Red dots indicate the FAL (b) Same as panel (a) except replacing $\log_{10}G$ with $\log_{10}\nu$.

5 Discussion

In this section, we discuss some key wave characteristics mentioned in the analysis, and the behaviors of calibrated model parameters. Some thoughts about wave-in-ice modeling are provided at the end.

5.1 Evolution of wave characteristics

The behaviors of $k_{r,dominant}$ and PSD in Figures 1 and 4 may come from multiple mechanisms. The decrease of $k_{r,dominant}$ towards the interior ice is in agreement with a similar study in the MIZ (Shen et al., 2018), as well as the lengthening of dominant wave periods reported in many field observations (e.g., Robin, 1963; Wadhams et al., 1988; Marko, 2003; Kohout et al. 2014; Collins et al., 2015). The phenomenon is commonly explained by the low pass filter mechanism in literature. That is, higher frequency waves are preferentially attenuated, thus the power spectrum peak shifts to longer waves. However, though this mechanism is supported by the increasing trend of k_i with increasing wavenumber before the FAL, it is insufficient to explain the observations after the FAL, where the k_i – k_r curve is practically flat (Figure 5) and the peak of PSD shifts toward lower k_r with increasing latitude (Figure 4). A downshift of wave energy towards lower wavenumber might also be related to nonlinear wave-wave interaction. Through which, spectral wave energy in the main wave frequency could transfer into the low-frequency components. How to quantify these mechanisms is still an open question with little data especially in pack ice, where the skills in observations are still developing. A piece of critical information is the relationship between the wave period and wave energy, especially in the region after the FAL. Monteban et al (2019) showed promising applications of overlapping SAR images separated by a sufficient time gap to obtain such information.

The attenuation rate obtained in this study (~10^{-5} m^2/s) against wavenumber shows a slightly increasing trend before the FAL, while nearly flat trend and lower after the FAL. Similar magnitude of attenuation is found in the MIZ in both Arctic and Antarctic as reported in previous studies in the same period range but larger for shorter periods (e.g., Meylan et al., 2014; Doble et al., 2015; Rogers et al., 2016; Cheng et al., 2017). The analysis of attenuation against wavenumber in section 3 is obtained for pairs of observations over relatively

Formatted: English (US)

Deleted: modelling

Deleted: commonly

Deleted: -k_r

Deleted: as

Deleted: increases

Deleted: Two other mechanisms also may cause a…

Deleted: the

Deleted: wave numbers. One is the change of dispersion relation, so that the wavelength grows deeper into the ice cover. The other is the…

Deleted: transfer between

Deleted: components

Deleted: move the

Deleted: in

Deleted: spectra

Deleted: ¶
Figure 5. Similar as Figure 3, two-dimensional histogram of k_i^m against k_r.¶

Deleted: slight

short distances (<60 km). In Appendix B, we present another method to determine the overall attenuation, similar to the analysis of the attenuation of the significant wave height shown in Stopa et al. (2018b). By analyzing wavenumber by wavenumber over the entire space where the SAR data covers, the apparent attenuation coefficient is obtained by fitting hundreds of data over long distances, ignoring the higher variation of ice thickness (0.01~0.3 m) and the shift of dominant wavenumber from the PSD curves. The results are shown in Appendix B, Figure B2. In some cases, we can even have negative values of this attenuation, meaning energy increases as the wave propagates. What we would like to emphasize by showing this result is that over a very long-distance ice condition can change significantly, in addition to nonlinear energy transfer and wind input/dissipation, thus long-distance spectral analysis may become difficult to interpret.

5.2 About model calibration

The covariance values of the calibrated viscoelastic parameters are greater than those found in grease/pancake ice using buoy data (Cheng et al. 2017). In processing the SAR data, there are many challenges to be dealt with. It is extremely difficult to separate 1) sea ice variability, 2) wave height variability, and 3) instrument variability (speckle and in-coherent SAR noise). All of these influence the variations we see in the wave spectral data. Still, the scatter of the spectral attenuation shown in Figure 3 is significant even after the filtering described in section 3.1. This data scatter results in a large range of calibrated model parameters. We believe that the scatter of calibrated G, ν in both WS and FS models could be narrowed down by reducing the uncertainty of measured attenuation data. We also believe that for the FS model the calibrated values and spread could be reduced by modifying the objective function (Eq. (6)) with an additional constraint on the wavenumber, which presently shows an extremely large range as shown in Figure S4. Regardless, the FS model needs much larger G, ν to produce attenuation rates comparable to the observed data. This is the case not only for the pack ice but also for the MIZ. When analyzing data from the Antarctic MIZ reported in Kohout and Williams (2013), and by further constraining $k_r = k_{ow}/1.7$, Mosig et al. (2015) obtained $G = 4.9 \times 10^{12}$Pa, $\nu = 5 \times 10^7$m^2/s. Though far below the present case, these values are still orders of magnitude above the intrinsic values measured from solid ice (Weeks and Assure, 1967). Meylan et al. (2018) discussed the attenuation behavior among different dissipative models by assuming small $|k_r - k_{ow}|$. Specifically, they showed that the FS model produced $k_i \approx \frac{\rho_{ice}(1+V)h^3}{6\rho_{water}g^6}\nu\sigma^{11}$ and the pure viscous case of WS model (i.e., Keller (1998)'s model) produced $k_i \approx \frac{4\rho_{ice}h}{\rho_{water}g^4}\nu\sigma^7$. The higher the power in σ, the higher ν is to match the measured k_i in the high period (low frequency) waves range. The FS model also naturally leads to large G. As shown in Mosig et al. (2015), inverting the dispersion relation shown in Eqs. (5a,c) gives $G - i\sigma\rho_i\nu = 6\frac{\rho_w\sigma^2 - gk\rho_w - hk\rho_i\sigma^2}{h^3k^5(1+V)}$. The leading term of which in small k_r yields $G \approx O(k_r^{-5})$.

Deleted: the

Deleted: distance

Deleted: 3m

Deleted: A2

Deleted: meaningless

Deleted: The mask used in determining qualified data used in this study was described in …

Moved up [2]: Stopa et al.

Formatted: Font colour: Auto

Deleted: (2018b).

5.3 Thoughts on modeling wave-ice interaction

Damping models play a crucial role in spectral attenuation. At present, to use any specific model to describe wave attenuation is tentative. The identified damping mechanisms are many. For instance, boundary layer under the ice cover (Liu and Mollo-Christensen, 1988; Smith and Thomson, 2019), spilling of water over the ice cover and interactions between floes (Bennetts and Williams, 2015; Herman et al., 2019a, b), jet formation between colliding floes (Rabault, 2019), have all been reported in laboratory or field studies. A full waves-in-ice model that considers all important mechanisms is not yet available. While theoretical improvements are needed to better model wave propagation through various types of ice covers, practical applications cannot wait. Calibrated models that are capable of reproducing key observations must be developed in parallel to model improvements. The present study provides a viable way to calibrate two such models available in WW3. These models lump all dissipative mechanisms in the ice cover into a viscous term. This type of model calibration studies has two obvious utilities. One, with proper calibration, models can capture the attenuation of the most energetic part of the wave spectrum. Two, the discrepancies may be used to motivate model development that includes missing mechanisms, thereby help future model development. Because different physical processes may play different roles under various ice morphology, collecting wave data to calibrate these models under various ice types is necessary. Finally, more observations with higher quality data will improve the modeling of the wave-ice interaction and the robustness of the models.

6 Conclusions

In this study, we use the wave spectra retrieved from SAR imagery to examine the spectral attenuation in young pack ice. These images were obtained in the Beaufort Sea on 12 October 2015. According to the analysis of data retrieved over several hundred kilometers, the observed decrease of wave energy and lengthening of dominant waves towards the interior ice are consistent with earlier in-situ observations. We investigate wave attenuation of dominant spectral densities per wavenumber between two arbitrary locations in the region separated by less than 60 km. Similar attenuation rates are observed for all wavenumbers from 0.019 to 0.045 m^{-1} (estimated wave period from 9 to 15 s). After isolating the ice induced attenuation out from these data, we calibrate two viscoelastic-type wave-in-ice models through an optimization procedure between the measured data and theoretical results. Both models can generally match the observed attenuation corresponding to the energetic portion of the wave spectra, with a large difference in dispersion (see wavenumber plots in Figure 6 and Figure S4). For the WS model, the calibrated shear modulus (viscous parameter) in the region beyond the first appearance of leads with thicker ice is slightly larger (smaller) than that of the region closer to the ice edge before the first appearance of leads. The resulting wavenumber is within 5% of that from the open water dispersion.

Wave-ice interaction is complicated due to many co-existing physical processes. At present no models have fully integrated all identified processes. The present study demonstrates a method based on measured data to calibrate existing models so that they can be applied to meet the operational needs. As the models improve,

Deleted: of modelling

Deleted: Identified

Deleted: clarifies

Deleted: different

Formatted: Font: Times New Roman, Font colour: Auto, Not Expanded by / Condensed by

Deleted: The

Deleted: were

Deleted: the

Deleted: predominant area

Deleted: in

Deleted: , further north of the grease/pancake ice region along the ship and buoy tracks

Deleted: We then use

Deleted: wave

Deleted: rates to

Deleted: on

Deleted: produced

Deleted: However, marine operations in the ice-covered seas need wave forecasts.

further calibration exercises may be performed accordingly. For example, the eddy viscosity model (Liu and Mollo-Christensen, 1988) attributed the wave attenuation entirely to the water body under the ice cover. This model is also included in WW3 as the switch IC2, with the eddy viscosity as a tuning parameter. The present analysis can also be used to calibrate that model or models that try to combine both dissipation from the ice cover and the eddy viscosity from the water beneath (e.g. Zhao and Shen, 2018). From a physical point of view, dissipative mechanisms may be present simultaneously inside the ice cover and the water body underneath. However, the calibration of complex models with multiple co-existing processes is a difficult task that requires a much more dedicated study.

We conclude by noting that high-resolution spatial data from remote sensing provide new opportunities to investigate the wave-ice interaction over a large distance and different ice types. However, details of ice types and temporal observations are in development. To reach a full understanding and thus a complete waves-in-ice model requires collaboration from observation and modeling efforts.

Appendix A

The definition of the first appearance of leads was introduced in Stopa et al. (2018b). Here we provide more details of the methodology used. The SAR sea surface roughness images in Figure 1 of Stopa et al. (2018b) are divided into 5.1x7.2 km subimages with a 50% overlap of adjacent subimages in the range-azimuth domain. Each subimage contains 512×512 pixels. The FAL location for each range-position is defined as the minimum azimuth position where large-scale ice features were detected. Detection of large-scale ice features is applied to each SAR subimage as the following. We first compute a one-dimensional spectrum of the SAR subimage to produce an image modulation spectrum. The spectrum is then normalized by the maximum energy contained in wavelengths from 100 to 300 m (the wavelength range of the dominant sea state for this event). When the ratio of the average of the normalized image spectra with wavelengths in the range of 600-1000 m and the dominant ocean-wave wavelength range from 160-220 m exceeds 0.8, we deem that there is a “large-scale” feature such as lead within the image. Figure A1 shows two representative examples of detecting ice leads from SAR images captured before and after the FAL. From the criterion above, there are no leads in the top case, but leads are found in the bottom case. Also notice the change in the probability distribution of the roughness: the mean value changes (lower in the non-lead case compared lead case) and the standard deviation (lower in the non-lead case compared to the lead case).

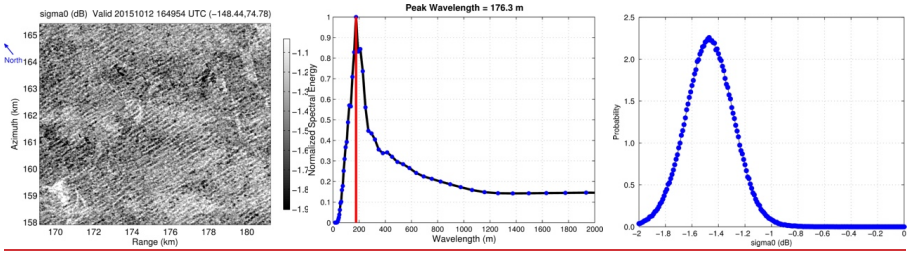

Deleted: which

Formatted: Not Highlight

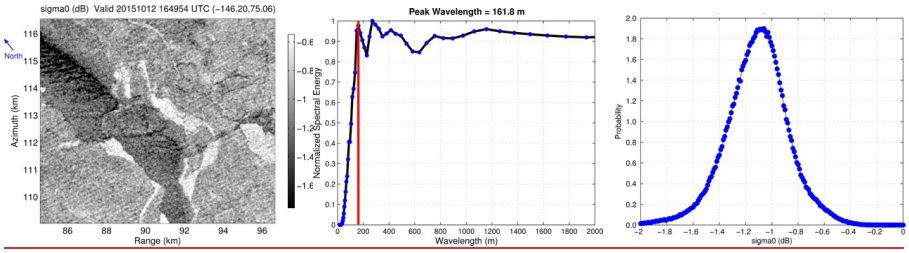

Figure A1. Illustration of the process to determine the FAL using two representative SAR subimages. (left) Surface SAR subimage roughness for a case located before the FAL (top) and a case located after the FAL. (middle) Normalized spectral energy (normalized by the maximum energy within the 100-300 m wavelengths) of the SAR subimages where the red line indicates the dominant wavelength. (right) The probability density function of the SAR roughness (backscatter or sigma0 of thermal noise in the SAR imagery) for the two cases.

Appendix B

We investigate the decay of the dominant energy component $E(k_r, \theta_{k_r})$ over a long distance along selected tracks with fixed longitude (145°W, 146°W, …, 150°W). Figure B1 shows $E(k_r, \theta_{k_r})$ (blue dots) collected within a given longitude interval 150 ± 0.1°W starting from 74.5°N towards the north. $E(k_r)$ for $k_r < 0.019$ m^{-1} is too scattered to show any attenuation trend. While as k_r increases, the data become tighter with a clear decay trend. To obtain attenuation coefficient $\alpha(k_r)$, we fit the $E(k_r, \theta_{k_r})$ by an exponential curve (black line) in each panel based on an exponential wave decay assumption.

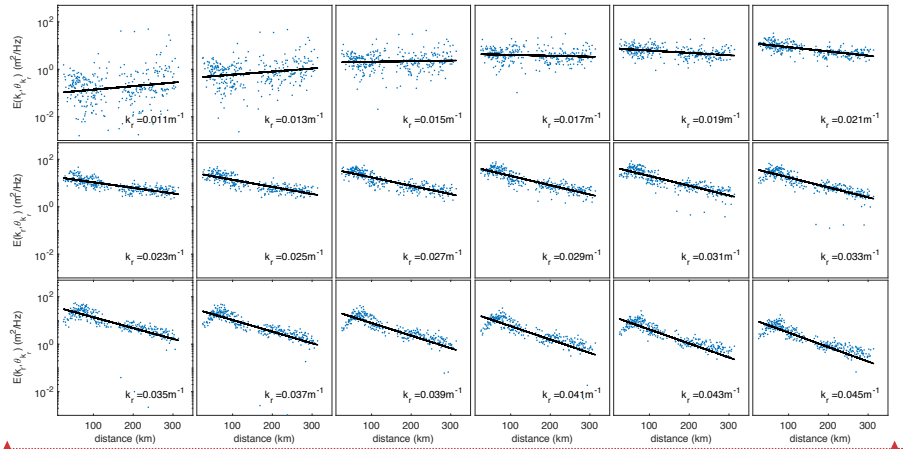

Figure B1. Evolution of dominant wave energy component over long distances at different wavenumbers. The horizontal axis is the distance along a longitude from 74.5°N towards the north.

Deleted: A1

Formatted: English (US)

Formatted: Not Highlight

Deleted: A1

Deleted: distance

Formatted: Not Highlight

The resulting $\alpha(k_r)$ against k_r is shown in Figure B2, as well as another five curves associated with different longitudes, processed in the same way. Figure B2 shows an increasing trend of $\alpha(k_r)$ against k_r as expected, and $\alpha(k_r$ <0.019 m^{-1}) are mostly negative. This method masks the variation of ice morphology and peak shifting of the power spectral density, thus it is insufficient to understand the damping mechanism in water-ice interaction. Hence, as our interest is to determine the attenuation in more consistent ice conditions, shorter distance between measuring points is adopted in section 3.

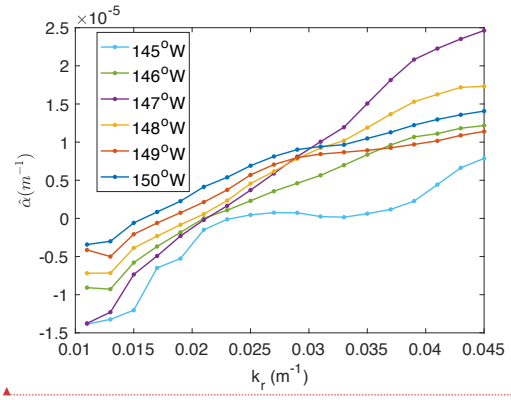

Figure B2. α against k_r of different longitude tracks.

Code and data availability

The code and data necessary to reproduce the results presented in this paper can be obtained from the corresponding author.

Author contribution

Stopa and Ardhuin retrieved the wave spectra dataset from SAR images. Cheng and Shen planned the research and prepared the manuscript with contributions from all authors. Cheng performed the analysis.

Competing interests

The authors declare that they have no conflict of interest.

Acknowledgements

The present work is supported by EU-FP7 project SWARP under grant agreement 607476, Office of Naval Research grant numbers N000141310294, N000141712862, and N0001416WX01117. Data, and a cruise

Deleted: A2
Deleted: A2
Deleted: While this plain
Deleted: blinds
Deleted: spectra
Deleted: the main body
Formatted: English (US)
Formatted: Not Highlight
Deleted: A2
Formatted: Not Highlight

report can be obtained at:https://drive.google.com/open?id=0B9Au2ZqQ-BM5YTJPWXBsV2Q0THc. The raw Sentinel-1A SAR data are provided by Copernicus and are available on-line via the Open Access Data Hub (https://scihub.copernicus.eu/). AMSR2 sea ice concentrations are from http://doi.org/10.5067/AMSR2/A2_SI12_NRT. SMOS sea ice thickness data are from https://icdc.cen.uni-hamburg.de/1/daten/cryo-sphere/l3c-smos-sit.html. CFSR wind data are from https://rda.ucar.edu/datasets/ds094.0/. OSCAR Current data are from https://www.esr.org/research/oscar/.

References

Ardhuin, F., Stopa, J., Chapron, B., Collard, F., Smith, M., Thomson, J., Doble, M., Blomquist, B., Persson, O., Collins III, C. O. and Wadhams P.: Measuring ocean waves in sea ice using SAR imagery: A quasi-deterministic approach evaluated with Sentinel-1 and in situ data, Remote sensing of Environment, 189, 211-222, 2017.

Ardhuin, F., Boutin, G., Stopa, J., Girard-Ardhuin, F., Melsheimer, C., Thomson, J., Kohout, A., Doble, M., and Wadhams, P.: Wave attenuation through an Arctic marginal ice zone on 12 October 2015: 2. Numerical modeling of waves and associated ice breakup, Journal of Geophysical Research: Oceans, 123, 5652-5668, 2018.

Bennetts, L. G., and Squire, V. A.: Model sensitivity analysis of scattering-induced attenuation of ice-coupled waves, Ocean Modelling, 45, 1-13, 2012.

Bennetts, L. G., and Williams, T. D.: Water wave transmission by an array of floating discs, Proceedings of the Royal Society A: Mathematical, Physical and Engineering Sciences, 471, 20140698, 2015.

Cheng, S., Rogers, W. E., Thomson, J., Smith, M., Doble, M. J., Wadhams, P., Kohout, A. L., Lund, B., Persson, O. P., Collins III, C. O., Ackley, C. F., Montiel F., and Shen H. H.: Calibrating a viscoelastic sea ice model for wave propagation in the Arctic fall marginal ice zone, Journal of Geophysical Research: Oceans, 122, 8770-8793, 2017.

Collins III, C. O., Rogers, W. E., Marchenko, A., and Babanin, A. V.: In situ measurements of an energetic wave event in the Arctic marginal ice zone, Geophysical Research Letters, 42, 1863-1870, 2015.

Collins III, C. O., Doble, M., Lund, B., and Smith, M.: Observations of surface wave dispersion in the marginal ice zone, Journal of Geophysical Research: Oceans, 123, 3336-3354, 2018.

Comiso, J. C., Parkinson, C. L., Gersten, R., and Stock, L.: Accelerated decline in the Arctic sea ice cover, Geophysical research letters, 35, 2008.

De Carolis, G., Olla, P., and Pignagnoli, L.: Effective viscosity of grease ice in linearized gravity waves, Journal of Fluid Mechanics, 535, 369-381, 2005.

Doble, M. J., De Carolis, G., Meylan, M. H., Bidlot, J. R., and Wadhams, P.: Relating wave attenuation to pancake ice thickness, using field measurements and model results, Geophysical Research Letters, 42, 4473-4481, 2015.

Formatted: English (UK), Pattern: Clear
Formatted: English (UK), Pattern: Clear
Formatted: English (UK), Pattern: Clear
Formatted: English (UK), Pattern: Clear
Formatted: English (UK), Not Highlight
Formatted: English (UK), Pattern: Clear
Formatted: English (UK), Pattern: Clear
Formatted: English (UK), Pattern: Clear
Formatted: English (UK), Pattern: Clear
Formatted: English (UK), Pattern: Clear
Formatted: English (UK), Pattern: Clear
Formatted: English (UK), Pattern: Clear
Formatted: English (UK), Pattern: Clear
Formatted: English (UK), Not Highlight
Formatted: English (UK), Pattern: Clear
Formatted: English (UK), Pattern: Clear
Formatted: English (UK), Pattern: Clear
Formatted: English (UK), Pattern: Clear
Formatted: English (UK), Pattern: Clear
Formatted: English (UK), Pattern: Clear
Formatted: English (UK), Pattern: Clear
Formatted: English (UK), Pattern: Clear
Formatted: English (UK), Pattern: Clear
Formatted: English (UK), Pattern: Clear
Formatted: English (UK), Pattern: Clear
Formatted: English (UK), Pattern: Clear
Formatted: English (UK), Pattern: Clear
Formatted: English (UK), Pattern: Clear
Formatted: English (UK), Not Highlight

Fox, C., and Haskell, T. G.: Ocean wave speed in the Antarctic marginal ice zone, Annals of Glaciology, 33, 350-354, 2001.

Hasselmann, S., and Hasselmann, K.: Computations and parameterizations of the nonlinear energy transfer in a gravity-wave spectrum. Part I: A new method for efficient computations of the exact nonlinear transfer integral, Journal of Physical Oceanography, 15, 1369-1377, 1985.

Hasselmann, S., Hasselmann, K., Allender, J. H., and Barnett, T. P.: Computations and parameterizations of the nonlinear energy transfer in a gravity-wave spectrum. Part II: Parameterizations of the nonlinear energy transfer for application in wave models, Journal of Physical Oceanography, 15, 1378-1391, 1985.

Johnsen, H., and Collard, F.: Sentinel-1 ocean swell wave spectra (OSW) algorithm definition. image, 1000, 500, 2009.

Herman, A., Cheng, S., & Shen, H. H.: Wave energy attenuation in fields of colliding ice floes–Part 1: Discrete-element modelling of dissipation due to ice–water drag. The Cryosphere, 13(11), 2019a.

Herman, A., Cheng, S., & Shen, H. H.: Wave energy attenuation in fields of colliding ice floes–Part 2: A laboratory case study. The Cryosphere, 13(11), 2901-2914, 2019b.

Keller, J. B.: Gravity waves on ice-covered water, Journal of Geophysical Research: Oceans, 103, 7663-7669, 1998.

Kohout, A. L., Williams, M. J. M., Dean, S. M., and Meylan, M. H.: Storm-induced sea-ice breakup and the implications for ice extent, Nature, 509, 604-607, 10.1038/nature13262, 2014.

Kohout, A. L., Williams, M. J. M., Toyota, T., Lieser, J., and Hutchings, J.: In situ observations of wave-induced sea ice breakup, Deep Sea Research Part II: Topical Studies in Oceanography, 131, 22-27, 2016.

Komen, G., Hasselmann, K., and Hasselmann, K.: On the existence of a fully developed wind-sea spectrum, Journal of physical oceanography, 14, 1271-1285, 1984.

Lange, M., Ackley, S., Wadhams, P., Dieckmann, G., and Eicken, H.: Development of sea ice in the Weddell Sea, Annals of Glaciology, 12, 92-96, 1989.

Liu, A. K., and Mollo-Christensen, E.: Wave propagation in a solid ice pack, Journal of Physical Oceanography, 18, 1702-1712, 1988.

Marko, J. R.: Observations and analyses of an intense waves-in-ice event in the Sea of Okhotsk, Journal of Geophysical Research: Oceans, 108, 2003.

MATLAB and Global Optimization Toolbox R2016a: The MathWorks Inc., Natick, Massachusetts, United States, 2016.

Meier, W. N., & Thomas, D. N.: Losing Arctic sea ice: observations of the recent decline and the long-term context. Sea ice, 290-303, 2017.

Meylan, M. H., Bennetts, L. G., and Kohout, A. L.: In situ measurements and analysis of ocean waves in the Antarctic marginal ice zone, Geophysical Research Letters, 41, 5046-5051, 2014.

Meylan, M. H., Bennetts, L. G., Mosig, J. E., Rogers, W. E., Doble, M. J., and Peter, M. A.: Dispersion relations, power laws, and energy loss for waves in the marginal ice zone, Journal of Geophysical Research: Oceans, 123, 3322-3335, 2018.

Formatted: , Pattern: Clear

Formatted: , Not Highlight

Formatted: English (UK), Pattern: Clear

Montiel, F., Squire, V. A., Doble, M., Thomson, J., and Wadhams, P.: Attenuation and directional spreading of ocean waves during a storm event in the autumn Beaufort Sea marginal ice zone, Journal of Geophysical Research: Oceans, 123, 5912-5932, 2018.

Monteban, D., Johnsen, H., & Lubbad, R.: Spatiotemporal observations of wave dispersion within sea ice using Sentinel-1 SAR TOPS mode. Journal of Geophysical Research: Oceans, 2019.

Mosig, J. E., Montiel, F., and Squire, V. A.: Comparison of viscoelastic-type models for ocean wave attenuation in ice-covered seas, Journal of Geophysical Research: Oceans, 120, 6072-6090, 2015.

Newyear, K., and Martin, S.: Comparison of laboratory data with a viscous two-layer model of wave propagation in grease ice, Journal of Geophysical Research: Oceans, 104, 7837-7840, 1999.

Rabault, J., Sutherland, G., Gundersen, O., and Jensen, A.: Measurements of wave damping by a grease ice slick in Svalbard using off-the-shelf sensors and open-source electronics, Journal of Glaciology, 63, 372-381, 2017.

Rabault, J., Sutherland, G., Jensen, A., Christensen, K. H., and Marchenko, A.: Experiments on wave propagation in grease ice: combined wave gauges and particle image velocimetry measurements, Journal of Fluid Mechanics, 864, 876-898, 2019.

Robin, G. d. Q.: Wave propagation through fields of pack ice, Philosophical Transactions of the Royal Society of London. Series A, Mathematical and Physical Sciences, 255, 313-339, 1963.

Rogers, W. E., Thomson, J., Shen, H. H., Doble, M. J., Wadhams, P., and Cheng, S.: Dissipation of wind waves by pancake and frazil ice in the autumn B eaufort S ea, Journal of Geophysical Research: Oceans, 121, 7991-8007, 2016.

Rosenblum, E., & Eisenman, I.: Sea ice trends in climate models only accurate in runs with biased global warming. *Journal of Climate*, *30*(16), 6265-6278, 2017.

Saha, S., Moorthi, S., Pan, H. L., Wu, X., Wang, J., Nadiga, S., Tripp, P., Kistler, R., Woollen, J., and Behringer, D.: The NCEP climate forecast system reanalysis, Bulletin of the American Meteorological Society, 91, 1015-1058, 2010.

Shen, H., Perrie, W., Hu, Y., and He, Y.: Remote sensing of waves propagating in the marginal ice zone by SAR, Journal of Geophysical Research: Oceans, 123, 189-200, 2018.

Shen, H. H., Ackley, S. F., and Hopkins, M. A.: A conceptual model for pancake-ice formation in a wave field, Annals of Glaciology, 33, 361-367, 2001.

Smith, M., Stammerjohn, S., Persson, O., Rainville, L., Liu, G., Perrie, W., Robertson, R., Jackson, J., and Thomson, J.: Episodic reversal of autumn ice advance caused by release of ocean heat in the Beaufort Sea, Journal of Geophysical Research: Oceans, 123, 3164-3185, 2018.

Smith, M., and Thomson, J.: Ocean surface turbulence in newly formed marginal ice zones, Journal of Geophysical Research: Oceans, 124, 1382-1398, 2019.

Snyder, R. L., Dobson, F. W., Elliott, J. A., and Long, R. B.: Array measurements of atmospheric pressure fluctuations above surface gravity waves, Journal of Fluid mechanics, 102, 1-59, 1981.

Formatted: English (UK)

Formatted: English (UK)

Formatted: English (UK), Pattern: Clear

Squire, V. A., Dugan, J. P., Wadhams, P., Rottier, P. J., and Liu, A. K.: Of ocean waves and sea ice, Annual Review of Fluid Mechanics, 27, 115-168, 1995.

Squire, V. A.: Of ocean waves and sea-ice revisited, Cold Regions Science and Technology, 49, 110-133, 2007.

Squire, V. A.: A fresh look at how ocean waves and sea ice interact, Philosophical Transactions of the Royal Society A: Mathematical, Physical and Engineering Sciences, 376, 20170342, 2018.

Squire, V.A. Ocean wave interactions with sea ice: a reappraisal. Ann. Rev. Fluild Mech. 52:37-60. https://doi.org/10.1146/annurev-fluid-010719-060301. 2020.

Stopa, J. E., Ardhuin, F., Chapron, B., and Collard, F.: Estimating wave orbital velocity through the azimuth cutoff from space-borne satellites, Journal of Geophysical Research: Oceans, 120, 7616-7634, 2015.

Stopa, J. E., Sutherland, P., and Ardhuin, F.: Strong and highly variable push of ocean waves on Southern Ocean sea ice, Proc Natl Acad Sci U S A, 115, 5861-5865, 10.1073/pnas.1802011115, 2018a.

Stopa, J., Ardhuin, F., Thomson, J., Smith, M. M., Kohout, A., Doble, M., and Wadhams, P.: Wave attenuation through an Arctic marginal ice zone on 12 October 2015: 1. Measurement of wave spectra and ice features from Sentinel 1A, Journal of Geophysical Research: Oceans, 123, 3619-3634, 2018b.

Stroeve, J., and Notz, D.: Changing state of Arctic sea ice across all seasons. Environmental Research Letters, 13(10), 2018.

The WAVEWATCH III® Development Group (WW3DG): User manual and system documentation of WAVEWATCH III® version 6.07. Tech. Note 333, NOAA/NWS/NCEP/MMAB, College Park, MD, USA, 465 pp. +Appendices, 2019.

Thomson, J., Ackley, S., Girard-Ardhuin, F., Ardhuin, F., Babanin, A., Boutin, G., Brozena, J., Cheng, S., Collins, C., Doble, M., …, and Wadhams, P.: Overview of the arctic sea state and boundary layer physics program, Journal of Geophysical Research: Oceans, 123, 8674-8687, 2018.

Wadhams, P., Squire, V. A., Goodman, D. J., Cowan, A. M., and Moore, S. C.: The attenuation rates of ocean waves in the marginal ice zone, Journal of Geophysical Research: Oceans, 93, 6799-6818, 1988.

Wang, R., and Shen, H. H.: Experimental study on surface wave propagating through a grease–pancake ice mixture, Cold Regions Science and Technology, 61, 90-96, 2010a.

Wang, R., and Shen, H. H.: Gravity waves propagating into an ice-covered ocean: A viscoelastic model, Journal of Geophysical Research: Oceans, 115, 2010b.

Weeks, W. F., and Assur, A.: The mechanical properties of sea ice, COLD REGIONS RESEARCH AND ENGINEERING LAB HANOVER NH, 1967.

Zhao, X., and Shen, H. H.: Wave propagation in frazil/pancake, pancake, and fragmented ice covers, Cold Regions Science and Technology, 113, 71-80, 2015.

Zhao, X., and Shen, H.H.: A three-layer viscoelastic model with eddy viscosity effect for flexural-gravity wave propagation through ice covers, Ocean Modelling, 151:15-23, 2018.

Formatted: English (UK), Pattern: Clear

Formatted: English (UK), Pattern: Clear

Formatted: English (UK), Pattern: Clear

Formatted: English (UK), Pattern: Clear

Formatted: English (UK), Pattern: Clear

Formatted: English (UK), Pattern: Clear

Formatted: English (UK), Pattern: Clear

Formatted: English (UK), Pattern: Clear

Formatted: Font: Not Italic, English (UK), Pattern: Clear

Formatted: English (UK), Pattern: Clear

Formatted: English (UK), Pattern: Clear

Formatted: Pattern: Clear

Page 5: [1] Deleted	Sukun Cheng	09/03/2020 05:10:00

Page 5: [2] Deleted	Sukun Cheng	09/03/2020 05:10:00